SnowPappus v1.0, a blowing-snow model for large-scale applications of Crocus snow scheme

Matthieu Baron[1,2], Ange Haddjeri[1], Matthieu Lafaysse[1], Louis Le Toumelin[1], Vincent Vionnet[3], and Mathieu Fructus[1]

[1]Univ. Grenoble Alpes, Université de Toulouse, Météo-France, CNRS, CNRM, Centre d'Études de la Neige, Grenoble, France
[2]Univ. Grenoble Alpes, Univ. Savoie Mont Blanc, CNRS, LECA, Grenoble, France
[3]Meteorological Research Division, Environment and Climate Change Canada, Dorval, QC, Canada

Correspondence: matthieu.baron@univ-grenoble-alpes.fr

Abstract. Wind-induced snow transport has a strong influence on snow spatial variability especially at spatial scales between 1 and 500 m in alpine environments. Thus, the evolution of operational snow modelling systems towards 100-500 m resolutions requires representing this process at these resolutions, over large domains and entire snow seasons. We developed SnowPappus, a parsimonious blowing snow model coupled to the state-of-the-art Crocus snow model able to cope with these requirements. SnowPappus simulates blowing snow occurrence, horizontal transport flux and sublimation rate at each grid cell as a function of 2D atmospheric forcing and snow surface properties. Then, it computes a mass balance using an upwind scheme to provide eroded or accumulated snow amounts to Crocus. Parameterizations used to represent the different processes are described in detail and discussed against existing literature. A point-scale evaluation of blowing snow fluxes was conducted, mainly at the *Col du Lac Blanc* observatory in French Alps. Evaluations showed SnowPappus performs as well as currently operational scheme SYTRON in terms of blowing snow occurrence detection, while the latter does not give access to a spatialized information. Evaluation of the simulated suspension fluxes highlighted a strong sensitivity to the suspended particle's terminal fall speed. Proper calibrations allow the model to reproduce the correct order of magnitude of the mass flux in the suspension layer. Numerical performances of gridded simulations of Crocus coupled with SnowPappus were assessed, showing the feasibility of using it for operational snow forecast at the scale of the entire French Alps.

1 Introduction

Mountainous areas in temperate regions usually experience a seasonal snowpack. Its physical properties, depth and persistence influence many local processes such as surface energy balance, soil temperature and vegetation productivity (Choler, 2015). They are critical to forecast and anticipate snow-related hazards, especially avalanche triggering (Schweizer et al., 2003; Morin et al., 2020a). On a larger scale, snow melt-out is an important source of water for downflow hydrological catchment, affecting water availability for agriculture and ecosystems, human consumption and hydropower (IPCC, 2022). Besides, the topographic complexity of mountainous environment promotes a huge snowcover spatial variability. Variations in elevation and aspect, by influencing air temperature and radiative incoming fluxes are major predictors of this variability at all scales.

However, these simple patterns are complexified by interaction between wind flow, precipitation patterns and various post-depositional processes (Mott et al., 2018). These interactions, among other phenomena, include orographic effects which tend to enhance precipitation on the windward side of mountain ranges (at a scale 10-100 km), interaction between wind flow and cloud formation processes and preferential deposition of snowfall at smaller scales (from dozens of meters to kilometers). Finally, at scales of meters to hundreds of meters, post-depositional processes, primarily wind-induced snow transport, have a big influence on snow depth and properties. This variability has consequences on the aforementioned processes, and thus must be taken into account when studying them.

During the last 40 years, numerous models have been developed to simulate snowpack evolution. They range from simple 1-layer models, often used in Global Climate Modelling or Numerical Weather Prediction (NWP) models to detailed multilayer snowpack models explicitly representing processes like snow metamorphism, compaction, etc. These detailed models include Crocus (Vionnet et al., 2012), SNTHERM (Jordan, 1991), SNOWPACK (Bartelt and Lehning, 2002). Crocus has been used for large-scale applications (Vernay et al., 2022; Vionnet et al., 2016) but only at a very coarse resolution, which prevents representing adequately snow spatial variability. In particular, it is currently used operationally for avalanche hazard forecasting in French mountains at a massif range scale. High resolution applications including wind-induced snow transport were limited to very small domains and/or short periods of time (Vionnet et al., 2014) due to computational costs and limited availability of high resolution forcing data.

However, growing computational power paves the way for moving large-scale operational systems towards resolutions of a few hundreds of meters, also sustained by the perspective of assimilation of promising high-resolution observations (Deschamps-Berger et al., 2022). It requires to represent phenomena driving snowpack variability at this scale, including pre-depositional processes, which are increasingly represented in non-hydrostatic atmospheric models up to kilometre resolution and post-depositional processes such as wind-induced snow transport, which can be included within the snowpack scheme. Regarding wind-induced snow transport, various modelling approaches have been developed for mountainous terrain including a fully explicit snow-atmosphere coupling (Vionnet et al., 2014; Sharma et al., 2021). However, this approach is not affordable in terms of numerical cost on large temporal and spatial scales, explaining the use of much simpler schemes in snow hydrology applications (Bowling et al., 2004; Pomeroy et al., 2007; MacDonald et al., 2009), associated with simpler snow models than Crocus.

In the above-mentioned context of increasing resolution of snow modelling systems, the long-term project of CNRM aims at performing simulations with Crocus at the scale of the French Alps at 250m resolution in an operational purpose, associated with a data assimilation framework requiring ensemble runs of 50-100 members (Largeron et al., 2020; Cluzet et al., 2021). The 250 m resolution allows a trade-off between the need for precisely representing slopes and aspects, influencing mass and energy balance of the snowpack, and the expected computational cost (Lafaysse, 2023; Baba et al., 2019). In this context, a numerically efficient representation of wind-induced snow transport that can be coupled to Crocus simulations is lacking while this is necessary to better account for its impact on avalanche forecasting over French mountains. Two blowing snow schemes coupled with Crocus exist yet : SYTRON (Vionnet et al., 2018) and Crocus-Meso-NH (Vionnet et al., 2014). However, both are unsuitable for this geometry and resolution.

Thus, the goal of this paper is to describe and present first evaluations of a novel blowing snow scheme, SnowPappus, coupled to Crocus and able to be included in the aforementioned large-scale simulation system. Point-scale evaluation of blowing snow flux will be presented to discuss the modelling choices. In order to avoid a prohibitive computational cost, this scheme shall not be much more computationally intensive than the Crocus model itself, and it will be forced with 2D wind fields downscaled from NWP systems rather than coupled with 3D high resolution atmospheric models.

A major interest in coupling Crocus with a blowing snow scheme is its detailed representation of snow stratigraphy and microstructure as it may be an opportunity for the simulation of snow transport occurrence (Guyomarc'h and Mérindol, 1998; Lehning et al., 2000). Therefore, we test the added value of microstructure-based parameterizations of snow transport occurrence in the evaluation section. Moreover, it allows Crocus to be used as a tool for avalanche forecasting (Morin et al., 2020b). Given that wind slabs formed by wind-induced snow deposition are one of the main causes of avalanche triggering (Schweizer et al., 2003), a blowing snow scheme coupled with Crocus could become a powerful tool for avalanche forecasting, even if evaluation of the simulated stratigraphy is out of the scope of this study.

The paper is organized as follows: Section 2 presents useful state of the art for blowing snow flux modelling in order to justify methodological choices for SnowPappus model, which is fully described Sect. 3. Section 4 presents the methods used to run and evaluate simulations. Section 5 and 6 finally present and discuss the results.

2 Blowing snow flux computation : state of the art

2.1 Blowing snow occurrence

Transport is initiated when the fluid shear stress exerted near the surface exceeds the weight of the grains and their cohesion force (Schmidt, 1980) which occurs above a threshold wind speed. In the case of snow, a threshold value U_t above which blowing snow occurs is commonly defined, although initiation and persistence of transport may require different wind speeds (Castelle et al., 1994; Michaux, 2003).

The threshold wind speed varies strongly as a function of snow properties, ranging from 4 $m.s^{-1}$ for freshly fallen snow to 15 ms^{-1} or even more for old refrozen or wet snow (Li and Pomeroy, 1997; Guyomarc'h and Mérindol, 1998; Clifton et al., 2006). The proposed parameterisations are based on temperature (Li and Pomeroy, 1997), snow density (Liston et al., 2007) or snow surface microstructural properties (Guyomarc'h and Mérindol, 1998; Raderschall et al., 2008). Formulations have been used to assess the threshold wind speed. Parameterizations based on snow surface properties (density or microstructure properties) allow a wider range of threshold wind speeds (typically from 4 to 12 m s^{-1} in Guyomarc'h and Mérindol (1998)) thanks to the discrimination between fresh and old snow.

However, they are consequently very sensitive to the simulated snow surface properties that can be highly uncertain (Helfricht et al., 2018) and not always measurable. Therefore, error compensation between the snow model and the parameterizations may exist. Parameterization of Guyomarc'h and Mérindol for SnowPappus has been extensively tested with Crocus (Vionnet et al., 2013, 2018).

2.2 Horizontal blowing snow fluxes

2.2.1 Notations and geometric considerations

In the following subsection, we discuss how the horizontal blowing snow flux can be estimated when transport occurs. We define c as the concentration of snow particles in the air (kg m^{-3}), u_p the horizontal speed of snow particles (m s^{-1}). Considering for simplicity the transport-related physical variables only depend on the height z, we can express the horizontal snow flux (kg m^{-2} s^{-1}) as $q(z) = u_p(z)c(z)$. Then, the integrated horizontal blowing snow flux can be obtained by $Q = \int q(z)dz$ (kg m^{-1} s^{-1}). Q represents the total mass of snow transported horizontally by units of length and time. In this paper, we use q for fluxes at a given height and Q for integrated fluxes.

2.2.2 Blowing snow particle trajectories and transport modes

When snow particles are detached from the snowpack, it is usually considered they are submitted only to gravity and drag force from the fluid (Bintanja, 2000; Kind, 1992), neglecting particle collisions and possible electrostatic interactions (Schmidt et al., 1999). Turbulent fluctuations of the drag force particles are exposed to is usually modelled as a turbulent diffusion process (Bintanja, 2000; Gallée et al., 2001; Vionnet et al., 2014; Sharma et al., 2021).

The trajectory of transported particles can exhibit different shapes, corresponding to different transport modes. In the limit case where turbulent diffusion has a negligible influence on the trajectory, a particle falls back on the snow cover after a single jump of a few centimeters, with possible rebounds. This corresponds to "saltation" transport. In the opposite case, when turbulent diffusion plays an important role, particles exhibit a random motion on the vertical axis, so-called "suspension" and can reach much higher elevations, from decimeters to hundreds of meters above the surface. However, both processes can be described with the same dynamic equations (Nemoto and Nishimura, 2004) and the transition between them is not clear, leading some authors to introduce "modified saltation" for intermediate trajectories (Shao, 2005; Nemoto and Nishimura, 2004). A third mode of transport, so-called reptation, has been described and corresponds to the rolling of big particles at the surface (Mott et al., 2018), but is often neglected (Pomeroy et al., 1993; Vionnet et al., 2014; Sharma et al., 2021, e.g.).

Furthermore, snow transport is complexified by possible fragmentation and sublimation of snow particles during transport, and by complex feedbacks on near-surface air flow (Melo et al., 2022; Comola and Lehning, 2017), snow surface properties (Vionnet et al., 2013), etc. Saltation in particular is still an open research topic, with still some recent fieldwork and experimental studies unravelling new saltation modes and mechanisms (Aksamit and Pomeroy, 2017; Mott et al., 2018).

2.2.3 Suspension transport modelling

Numerous models with different degrees of complexity have been developed in order to simulate the air-blowing snow mixture. The most comprehensive ones represent both saltation and suspension by coupling a Computational Fluid Dynamics model with the simulation of individual particles motion and interaction with the snow bed in a lagrangian mode (Nemoto and Nishimura, 2004; Groot Zwaaftink et al., 2014; Melo et al., 2022).

In order to deal with real-case applications, simplified models have been developed. In the latter, snow concentration in the suspension layer is computed in an eulerian mode, the lower boundary condition being given by a semi-empirical representation of saltation. The equations governing particle concentrations usually include an advection term driven by the mean flow field, a sedimentation term, a diffusion term supposed to account for the effect of turbulent diffusion motion and a sink term accounting for sublimation. The most complete of these models like MAR (Gallée et al., 2001), Crocus-MesoNH (Vionnet et al., 2014), SnowDrift3D (Schneiderbauer and Prokop, 2011a) and CryoWRF (Sharma et al., 2021) are included within a 3D atmospheric model and solve an equation of the following form, with sometimes refinements to account for blowing snow particle size distributions influence on the concentration profile (Bintanja, 2000; Déry and Yau, 1999; Vionnet et al., 2014; Déry and Yau, 2001; Yang and Yau, 2008; Pomeroy et al., 1993; Marsh et al., 2020) which are not presented here for simplicity.

$$\frac{\partial c}{\partial t} + (\mathbf{U}(\mathbf{x},\mathbf{t}).\nabla)c = \nabla.(K_{\text{snw}}(\mathbf{x},t)\nabla c(\mathbf{x},t)) - v_f \frac{\partial c}{\partial z} - s \tag{1}$$

with K_{snw} the turbulent diffusion coefficient of snow particles ($\text{m}^2\ \text{s}^{-1}$), $\mathbf{U}$ the wind speed (m s^{-1}), v_f the terminal fall speed of snow particles (m s^{-1}) and s the sublimation rate ($\text{kg m}^{-3}\ \text{s}^{-1}$).

This equation can be simplified by being solved with a stationary state assumption and using a simplified wind profile (Marsh et al., 2020), or even reduced to a one-dimensional and stationary form by neglecting the effect of horizontal heterogeneity of wind speed on the concentration profile, like in Prairie Blowing Snow Model (Pomeroy et al., 1993; Pomeroy and Male, 1992) and SnowTran3D (Liston and Sturm, 1998). A possible form of the equation is then :

$$\frac{\partial c}{\partial z}(K_{\text{snw}}(z)\frac{\partial c}{\partial z}) + v_f \frac{\partial c}{\partial z} + s(z) = 0 \tag{2}$$

Several authors use additional hypotheses (Gordon et al., 2009) : (i) influence of sublimation on the suspension concentration profile is neglected (ii) The diffusion coefficient of snow is proportional to the diffusion coefficient of momentum K_{sca}, leaving $K_{\text{snw}} = \frac{K_{\text{sca}}}{\zeta}$ with ζ a dimensionless quantity so called the Schmidt number (Vionnet, 2012; Naaim-Bouvet et al., 2010). Assuming a neutrally stable stratified flow, $K_{\text{snw}} = \frac{k u_* z}{\zeta}$. (iii) The net flux of particles from the snow surface is assumed to be negligible. Note Eq. 1 assumes also all snow particles have the same terminal fall speed. With these 4 hypotheses, it can be shown the concentration profile in the suspension layer follows a power-law (Gordon et al., 2009; Naaim-Bouvet et al., 2010):

$$c(z) \propto z^{-\gamma} \text{ with } \gamma = \frac{\zeta v_f}{k u_*} \tag{3}$$

Despite the strong assumptions necessary to obtain this power-law profile, it has been used successfully to fit observed concentration profiles (Guyomarc'h et al., 2019; Vionnet, 2012; Gordon et al., 2009; Mann et al., 2000).

The concentration profile in the suspension layer, and thus the flux in the suspension layer, depend strongly on the γ exponent, itself depending on the terminal fall speed and the Schmidt number. However, the only direct field measurement of blowing snow terminal fall speed was performed by Takahashi (1985) in Antarctica. Estimations of ζ are indirect and mostly rely on concentration profile analysis (Vionnet, 2012; Naaim-Bouvet et al., 2010). They might be affected by several phenomena such as turbulent kinetic energy destruction, incorrect estimation of v_f, etc. Thus, it is easier to rely on direct estimations of the γ exponent from field observations of concentration profiles rather than estimating it from the physical parameters ζ and v_f. An

effective terminal fall speed $v_f^* = \gamma k u_*$ can be defined. Analysis of concentration profile at *Col du Lac Blanc* in the French Alps and in Antarctica (Vionnet, 2012) at height of 0.1 - 1 m, as well as v_f measurements from Takahashi (1985) suggest that (i) observed v_f^* or v_f have a large variability and range from 0.2 to 1.0 m s^{-1} (ii) a "recent snow" and "old snow" regime are distinguished, v_f^* increasing with snow age (iii) v_f^* increases with wind speed, at least in the case of recent snow. In this latter case v_f^* fits correctly with Naaim-Bouvet et al. (1996) parameterization. Possible theoretical explanations for these trends include differences in shape between old and fresh snow particles, and the ability of stronger winds to make bigger particles enter in suspension. These studies considered snow was recent either during a precipitation event (Takahashi, 1985; Vionnet, 2012) or when it was aged less than one day.

2.2.4 Lower boundary condition for suspension transport

In most blowing snow models, the transition between saltation and suspension layer is treated assuming the height of the saltation layer can be defined, and that the particle concentration at the top can be used as a lower boundary condition for the suspension layer. However, detailed saltation models (Melo et al., 2022; Nemoto and Nishimura, 2004) indicate that (i) there is a change in the decay rate with height of snow particles concentration in the transition zone (ii) a bimodal particle size distribution is observed in the transition zone, with one mode associated with the biggest particles vanishing above the transition zone, and the other mode associated with the smallest particles vanishing under it. Nemoto and Nishimura (2004) argue that in this transition zone, the smallest particles are yet in suspension whereas the biggest are still in a saltation motion. This suggests not all saltating particles are able to enter the suspension state, with only the smallest ones being picked up. Thus, we argue particle concentration at the top of the saltation layer cannot be simply taken as a boundary condition, as it is still a transition zone where part of particles are in saltation motion, without significant effect of turbulent diffusion on their trajectories, and another part in suspension motion. The upper height of this transition zone can be estimated at 12-14 cm from Melo et al. (2022) results. In the absence of precise information on this transition zone, the lower boundary condition for suspension transport should preferably be extrapolated from concentration measurements in the suspension layer rather than from estimation of the concentration in the saltation layer.

Pomeroy and Male (1992) fitted field-observed suspension flux and showed $c(h^{P92}) = c_{\text{salt}}^{\text{P90}}$ is a suitable boundary condition to simulate fluxes in the suspension layer, with $c_{\text{salt}}^{\text{P90}}$ the concentration predicted by the saltation model of Pomeroy and Gray (1990) which is detailed in the following subsection, and $h^{P92} = a \times u_*^{1.27}$ with a = 0.0834 $\text{m}^{-0.27}$ $\text{s}^{1.27}$. However, h^{P92} is clearly located in the transition zone between saltation and suspension, so the concentration profile predicted by this model under 10-15 cm must be seen as an extrapolation of suspension behaviour.

2.2.5 Simple saltation models

Simple semi-empirical parameterizations have been developed to simulate the flux and concentration of blowing snow in the saltation layer. Two of them, which were used in distributed snow transport models, will be compared in detail in the following :

– Parameterization of Pomeroy and Gray (1990) (P90):

$$Q_{\text{salt}}^{P90} = h_{\text{salt}}^{P90} u_p c_{\text{salt}}^{\text{P90}} = A \frac{\rho_{\text{air}}}{u_* g} u_t^* (u_*^2 - u_t^{*2}) \tag{4}$$

$$\text{with } h_{\text{salt}}^{P90} = 1.6 \frac{u_*^2}{2g} \tag{5}$$

With Q_{salt}^{P90} the integrated saltation flux, h_{salt}^{P90} an estimation of the height of the saltation layer, ρ_{air} the air density (kg m^{-3}), $A = 0.68$m s^{-1} an empirical constant, u_t^* the threshold friction velocity and $u_p = 2.8 u_t^*$ the snow particle velocity. This formulation was widely used without modifications or further test in blowing snow models (Pomeroy et al., 1993; Liston and Sturm, 1998; Bintanja, 2000; Gallée et al., 2001; Marsh et al., 2020).

– Parameterization of Sørensen (2004) - Vionnet (2012) (S04):

$$Q_{\text{salt}}^{S04} = \frac{\rho_{\text{air}} u_*^3}{g} (1 - V^{-2})(a + bV^{-2} + cV^{-1}) \tag{6}$$

with $V = \frac{u_*}{u_{*t}}$ and a, b and c calibration parameters (Sørensen, 2004). They were calibrated as $a = 2.6$, $b = 2.5$ and $c = 2$ in the case of snow (Vionnet, 2012). It was used in the coupling of Crocus with MesoNH (Vionnet et al., 2014).

P90 and S04 give very different results, S04 predicts a higher flux by a factor of about 10, as highlighted by several authors (Melo et al., 2022; Doorschot and Lehning, 2002). Despite a physical basis, P90 and S04 are calibrated on measurements, from terrain observations in the case of P90 in various conditions (and in particular wind speeds), and from a wind tunnel experiment in the case of S04, conducted on a single, non-cohesive, snow type, at a single wind speed and air temperature (Nishimura and Hunt, 2000). Thus P90 seems to have better empirical support than S04. However, measurements carried out to calibrate P90 suffer high uncertainties, in particular concerning their height (Pomeroy and Gray, 1990), and more complex saltation models support the magnitude of S04 predictions (Doorschot and Lehning, 2002; Melo et al., 2022).

Numerical and experimental works supporting S04 use snow fluxes integrated up to 10-15 cm (Nishimura and Hunt, 2000; Melo et al., 2022) whereas P90 formulation is supposed to represent a flux between 0 and h_{salt}^{P90} which is typically 1-4 cm in the range of speed explored in the experiments of Pomeroy and Gray and Nishimura and Hunt. Thus, we argue that Q_{salt}^{S04} represents not only the saltation transport but also all the transition zone towards suspension transport, whereas Q_{salt}^{P90} gives only the flux at the base of the saltation layer. Thus, both formulations cannot be compared directly.

3 Model description

3.1 Crocus description

Crocus (Vionnet et al., 2012; Carmagnola et al., 2014) is a detailed multilayer snow scheme in which each snow layer is characterized by its mass, density, age, liquid water content, a historical variable stating if the layer has experienced liquid water in the past and microstructural properties: the optical diameter D_{opt} and the sphericity s. These properties evolve in time by the representation of all main physical processes (heat diffusion and phase changes in relation with each layer energy budget, metamorphism, liquid water percolation, compaction).

3.2 Blowing snow occurrence

Consistent with Section 2.1, we assume snow transport occurs when the wind friction velocity exceeds a threshold friction velocity u_t^* depending on the properties of the surface snow layer. Three cases are distinguished: (i) Following Vionnet et al. (2013), if the layer contains or had formerly contained liquid water, the snow is considered as non-transportable. (ii) In the case of dry snow older than 1 hour, we use a threshold wind speed which can depend on snow microstructure. Two options were implemented:

- The default option GM98 : u_t^* is calculated as a function of snow microstructure using the parameterization of Guyomarc'h and Mérindol (1998).

$$u_t^* = k\frac{U_t}{\log(\frac{h_{\text{ref}}}{z_0})} \tag{7}$$

$$\text{with } U_t = \begin{cases} 0.75d - 0.5s + 0.5 \text{ for dendritic snow} \\ -0.583g_s - 0.833s + 0.83 \text{ for non-dendritic snow} \end{cases} \tag{8}$$

$$\tag{9}$$

  whith U_t the wind velocity at a reference height h_{ref}=5 m. d, s and g_s are the dendricity, the sphericity and the grain size, which were the variables used to describe snow microstructure in the oldest versions of Crocus. They can be expressed as a function of sphericity and optical diameter D_{opt} (see appendix D)

- Option CONS : Threshold friction velocity is constant for snow older than one hour.

(iii) If the snow layer age is inferior to 1 hour, we again follow Vionnet et al. (2013) fixing U_t^{5m} to 6 m s^{-1} during snowfall events, in agreement with wind tunnel experiments of Sato et al. (2008).

Eq. 8 is very sensitive to the initial microstructure properties of falling snow, related to wind speed following(Vionnet et al., 2012).

As the parameterization of Guyomarc'h and Mérindol (1998) is not valid during snowfall, the main novelty introduced in SnowPappus is a modified value of U_t during snowfall, representing the weaker cohesion of ice bonds in new snow. This approach differs from Vionnet et al. (2013) who instead adjusted falling snow properties without modification of U_t.

Comparative evaluation of the two techniques will be presented in the next section. Note that this hypothesis leads to an instantaneous increase of the threshold wind speed when snow age reaches 1 h.

3.3 Horizontal blowing snow flux

3.3.1 Suspension transport

To define a model suitable for our large-scale application, a trade-off between model complexity and accuracy was necessary. The numerical cost of fully coupled models prevents their use for our target domains and resolution. Besides, two-dimensional

wind speed input may limit the added value of three-dimensional solving of advection-diffusion equation (Eq. 1). Finally, the target resolution (250 meters) is close or even bigger than the topographic scales able to stop or enhance transport. As a consequence, the effects of subgrid variability of the wind field may dominate the effects of its resolved variability between grid cells. All these reasons led us to choose to solve the simple 1D advection-diffusion equation, as this approximation may not be the limiting factor for model uncertainty at our target resolution.

For simplicity, we assume a neutrally stable and stratified flow, with the well-known logarithmic wind speed profile.

$$U(z) = \frac{u_*}{k} \ln(\frac{z}{z_0}) \tag{10}$$

with U the horizontal wind speed (m s^{-1}), u_* the wind friction velocity (m s^{-1}) and z the height above snow surface (m), k the Von Karman's constant (dimensionless), found empirically to be equal to 0.41 and $z_0 = 1.10^{-3}m$ the roughness length of the surface (m). Knowing wind speed at a reference height z_{forc}, we deduce u_* by inverting equation 10. We use a constant roughness height $z_0 = 1.10^{-3}m$, which is the default SURFEX value for snow.

Following the 4 hypotheses described Sect. 2.2.3, we use the power-law profile to describe the particle concentration in the suspension layer, taking additionally the following lower boundary condition :

$$c(z_r) = c_r \tag{11}$$

with z_r a reference height (m) and c_r a reference concentration (kg m^{-3}), which will be detailed in Sect. 3.3.2. Then we have :

$$c(z) = c_r(\frac{z}{z_r})^{-\gamma} \text{ with } \gamma = \frac{v_f^*}{k u_*} \tag{12}$$

with v_f^* the effective terminal fall speed described Sect. 2.2.3.

In suspension motion, snow particles are embedded in the atmospheric turbulent air flow, consequently simple suspension models assume their horizontal mean velocity $u_p(z)$ is equal to wind speed $U(z)$ (Marsh et al., 2020; Liston and Sturm, 1998; Pomeroy and Gray, 1990). We also use this hypothesis in our work.

With all these elements, we can express the total suspension snow flux as :

$$Q_{t,int} = \int_{h_{\text{susp}}}^{h_{\text{max}}} q_{\text{susp}}(z)dz = \frac{c_r z_r u_*}{k(1-\gamma)}[(\frac{h_{\text{max}}}{z_r})^{-\gamma+1}(\log(\frac{h_{\text{max}}}{z_0}) - \frac{1}{1-\gamma}) - (\frac{h_{\text{susp}}}{z_r})^{-\gamma+1}(\log(\frac{h_{\text{susp}}}{z_0}) - \frac{1}{1-\gamma})] \tag{13}$$

with h_{susp} the minimum height of the suspension layer and h_{max} is the maximum height of the suspension layer. Following Pomeroy and Male (1992), we use $z_r = h^{P92}$ and $c_r = c_{\text{salt}}$ (defined Sect. 2.2.4 and 2.2.5). Parameterizing v_f and ζ is necessary to compute Q_{susp} and will be the object of the following paragrah.

Fetch distance influences suspension transport by limiting the height suspended particles can reach. Here, we follow Pomeroy et al. (1993) and consider $h_{\max}$ grows with the fetch distance l_{fetch} (distance after a slope break or an obstacle preventing transport). This strong approximation of an abrupt fall of particle concentration above h_{max} has generally little influence on

the flux computation, except at very high wind speeds when the flux profile becomes non-integrable. More details on that topic are given in Appendix B.

In order to parameterize v_f^*, we define from Vionnet (2012) observations $v_{f,old}^* = 0.8$ m s^{-1} and $v_{f,fresh}^* = \min(0.38u_* + 0.12, 0.8$ m s$^{-1})$ (parameterization from Naaim-Bouvet et al., 1996). Then, in SnowPappus, the effective terminal fall speed is set to :

$$\begin{cases} v_f^* = & v_{f,\text{fresh}}^*(u_*) & \text{if } d > 0 \text{ and } A < 0.05 \text{ days} \\ v_f^* = & v_{f,\text{old}}^* & \text{if } d = 0 \\ v_f^* = & v_{f,\text{old}}^*(1-F) + v_{f,\text{fresh}}^* F & \text{otherwise} \end{cases}$$

with A the age of the surface snow layer and $F = \min(1, \frac{d}{d_m})$ where d is the dendricity of the snow surface layer (Vionnet et al., 2012; Carmagnola et al., 2014). Our distinction between 'old' and 'fresh' regimes is arbitrary. We are always in the fresh snow case during a precipitation event, and move to the old snow regime more or less fast depending on d_m. This adjustable quantity is set by default to 0.5 (dimensionless), as the result of calibration on *Col du Lac Blanc* data, its sensitivity is assessed in the following evaluations (Sect. 4.3).

3.3.2 Saltation transport and transition with suspension

In the following subsection, we present how to compute the transport flux in the region under 10-15 cm height where the transport is a priori not pure suspension. It includes the saltation layer and the so-called "transition zone".

To overcome this difficulty, in the following, we note Q_{inf} the blowing snow flux integrated up to a height of $h_{susp} = 10-15$ cm (15 cm in the final code) and Q_{inf}^* its value at an infinite fetch distance (see below). We include in SnowPappus two methods to compute it, based respectively on P90 and S04 saltation models:

- **S04** : $Q_{\text{inf}^*} = Q_{\text{salt}}^{S04}$ (Eq. 6)
- **P90 + SnowPappus** : We separate the lower atmosphere into two sublayers (1) between snow surface and h^{P92} (defined in Sect. 2.2.4, used for the lower boundary condition for suspension) (2) between h^{P92} and h^{susp}. In layer 1, we consider the behaviour of Pomeroy and Gray (1990) can be applied, so that the speed of snow particles is $u_p = 2.8u_{*,t}$ and $c = c_{salt}^{P90}$(Eq. 4). In layer 2, the SnowPappus suspension behaviour is extrapolated, with $u_p = U(z)$ and c follows Eq. 12. Thus the flux integrated between the surface and h_{susp} is computed by:

$$Q_{\text{inf}^*} = Q_1 + Q_2 \tag{14}$$

$$Q_1 = \int_0^{h^{P92}} c_{\text{salt}}^{P90} u_p^{P90} dz = Q_{\text{salt}}^{P90} \frac{h^{P92}}{h_{salt}^{P90}} \tag{15}$$

$$Q_2 = \int_{h^{P92}}^{h_{\text{susp}}} c(z)U(z)dz \text{ with } c(z) = c_{\text{salt}}^{P90} (\frac{z}{h^{P92}})^{\frac{-v_f^*}{ku_*}} \tag{16}$$

Both methods are represented schematically in Fig. 1, and their outputs will be compared Sect. 5.1.

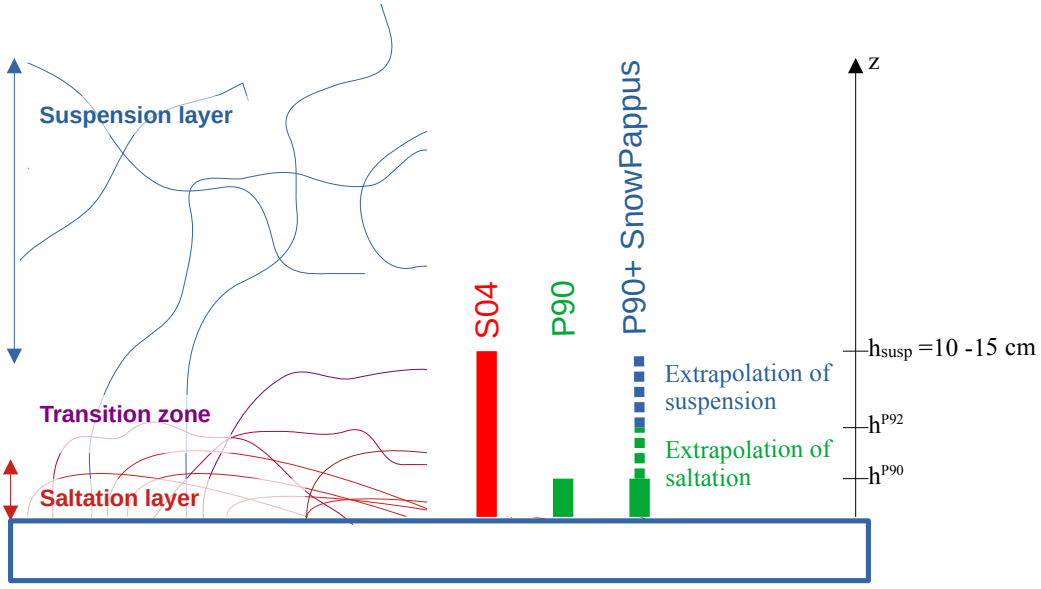

Figure 1. Schematic representation of the suspension and saltation layers and of the transition zone between them. The part of fluxes computed by the two saltation models S04 and P90 are represented schematically, as well as the 'P90+ SnowPappus' method, combining the P90 saltation model and the SnowPappus suspension model.

Most blowing snow models finally alter snow saltation fluxes considering the increasing relationship between flux and fetch distance (Pomeroy et al., 1993; Liston and Sturm, 1998; Bowling et al., 2004; Marsh et al., 2020). We follow this literature and use the parameterization proposed in SnowTran3D (Liston and Sturm, 1998). We consider $Q^*_{\text{inf}} = Q_{\text{inf}} f(l_{\text{fetch}})$ and $c_{salt} = f(l_{\text{fetch}}) c^{P90}_{salt}$ with $f(l_{\text{fetch}}) = (1 - \exp(-3\frac{l_{\text{fetch}}}{l^*}))$. $l^* = 500$ m represents the fetch length at which the saltation flux reaches 95% of its steady state value (Pomeroy et al., 1993).

Figure 2 shows the influence l_{fetch} has on the total transport flux , which is very strong in the first hundreds of meters. In mountainous environment, we can expect typical fetch distance to be in this range, and mostly inferior to our resolution (250 meters). We chose for simplicity to use by default a constant fetch distance on the whole grid $l_{fetch} = 250m$, which is a strong hypothesis. Different methods and algorithms exist to compute fetch in complex topographies (Bowling et al., 2004; Marsh et al., 2020) and could be included in a future version of SnowPappus.

3.4 Sublimation

Two different parameterizations of blowing snow sublimation rate q_{subl} (kg m^{-2} s^{-1}) were implemented in SnowPappus with default choice to Simplified Blowing Snow Model (SBSM) parameterization Essery et al. (1999).

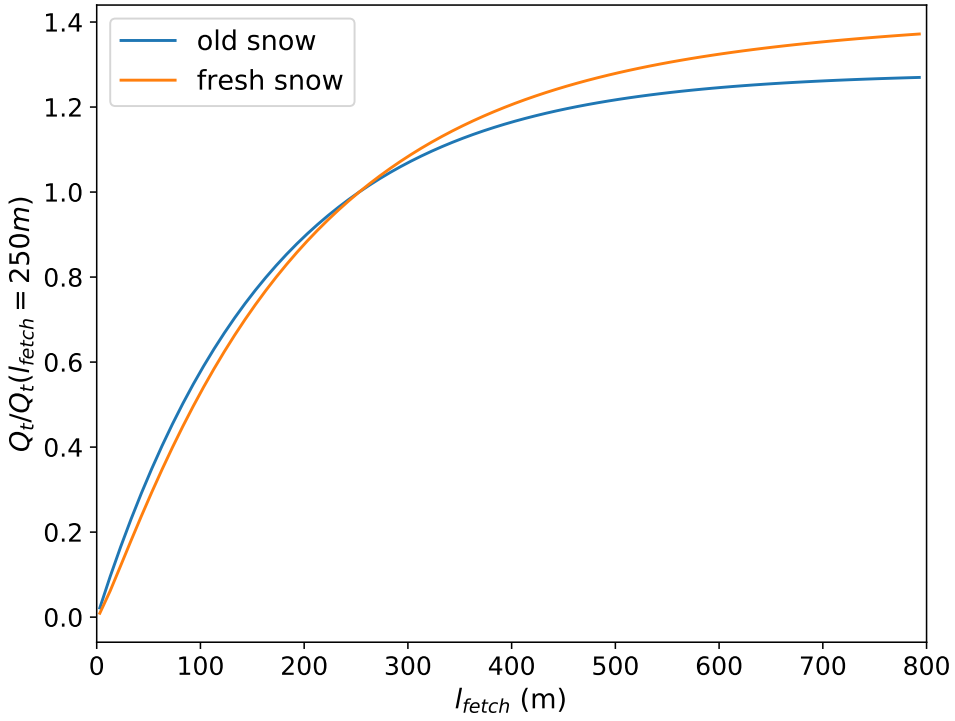

Figure 2. ratio between the total modelled transport rate Q_t and its value for the default fetch value $l_{fetch} = 250m$, as a function of fetch distance. The case of fresh snow, i.e. dendritic snow with here $u_{*t} = 0.27$ m s^{-1} (orange curve) and old snow, i.e. non-dendritic snow with here $u_{*t} = 0.39$ m s^{-1} (blue curve) are compared, both for a wind friction velocity of 0.6 m s^{-1} (which corresponds to approximately to a 2-m wind speed of 12 m s^{-1})

The first is an implementation of the SBSM parameterization from Eq.6 of Essery et al. (1999) and the SBSM documentation:

$$q_{subl} = \frac{\mu_{satc} \times 137.6}{F(T)} \times \frac{{u_{wind}}^5}{25000} \tag{17}$$

with F(T) expression given in appendix C function and μ_{satc} the under-saturation.

The second is from Eq.9 of Gordon et al. (2006) :

$$q_{subl} = A \left(\frac{T_0}{T_a}\right)^4 U_t \rho_a q_{si} \mu_{satc} \left(\frac{U}{U_t}\right)^B, \quad \text{for} \quad U > U_t \tag{18}$$

with q_{si} the saturation specific humidity, ρ_a (kg m^{-3}) the air density, U and U_t (m) wind and 5 meters wind threshold for transport at 5m ,A = 0.0018 and B=3.6 .

3.5 Mass balance

This section describes how SnowPappus simulates mass exchanges between neighbouring grid cell, once the amount of horizontal transport flux has been computed for each pixel. The snow transport direction is the same as the wind direction. Therefore, the problem simplifies as solving the mass balance equation. We define $Q_t = Q_{\text{inf}} + Q_{\text{susp}}$ as the total vertically integrated horizontal blowing snow flux (kg m^{-1} s^{-1}). The mass balance can be solved using the following continuity equation:

$$q_{dep}(x,y,t) = \nabla.Q_t(x,y,t) - q_{subl}(x,y,t) \tag{19}$$

with q_{dep} (kg m^{-2} s^{-1}) the pixel snow deposition, q_{subl} (kg m^{-2} s^{-1}) the snow transport sublimation and $\nabla.Q_t$ the total snow transport flux divergence. All these quantities are expressed *by sloping snow surface unit*. Indeed, Within SURFEX grid configuration, each grid point has a defined slope angle θ, and it is considered each grid cell has a ground surface $\frac{l_{\text{res}}^2}{\cos(\theta)}$ with l_{res} the grid horizontal resolution (m). In order to preserve mass balance of the domain, at a given point we assume:

$$\nabla.Q_t = (\nabla.Q_t)_{\text{flat}}\cos(\theta) = (\sum_{faces} \frac{Q_{t,in}(x,y,t)}{l_{\text{res}}} - \sum_{faces} \frac{Q_{t,out}(x,y,t)}{l_{\text{res}}})\cos(\theta) \tag{20}$$

with $(\nabla.Q_t)_{\text{flat}}$ the flux divergence computed as it would be on a perfectly flat terrain (kg m s^{-2}.

$(\nabla.Q_t)_{\text{flat}}$ can be expressed as the sum of the total snow transport flux Q_t leaving and entering the grid cell (in and out) by surface unit. The SnowPappus model uses a regular cartesian mesh grid discretization with cell-centred storage. This means each simulation point is regularly disposed on the simulation zone with each simulation point representing a squared pixel of fixed size. Our mesh grid being cell centred, we do not compute the transport fluxes at the pixel faces, as needed for the continuity equation 20. To obtain these values, an upwind scheme (Patankar, 2018) has been implemented, i.e. the zonal and meridian components of the fluxes at the face are assumed to be equal to the zonal and meridian flux computed at the center of the upwind pixels (in both directions):

$$Q_t(i,j,t) = Q_t(i \pm \frac{1}{2}, j \pm \frac{1}{2}, t) \tag{21}$$

with i,j being the grid coordinates of the center of pixels and $i \pm \frac{1}{2}$,$j \pm \frac{1}{2}$ pixel's border, as illustrated by Fig. 3.

This scheme was preferred to a linear interpolation of fluxes because it simplifies the mass balance closure in preventing snow mass creation. In our use case, the linear interpolation method would need extra steps with "gradient limiters" to ensure this (Greenshields and Weller, 2022) . Besides, the effect of fetch on the transport flux may cause the flux to respond to the change in the wind and snowpack conditions with a lag of a few hundred meters, the same order of magnitude as a grid cell.

We consider a given grid cell, on which local horizontal transport rate is written $Q_{t,\text{out}}$. We consider the four neighbouring cells located respectively north, south, west and east of the cell. We call $Q_{t,i}$ with $i = 1, \cdots, 4$ the horizontal transport rates on these cells, and call $\overrightarrow{n_i}$ the unitary normal vector going in the corresponding direction. With the upwind numerical scheme to obtain the pixel face crossing values, we obtain the following continuity equation for our SnowPappus model :

$$(\nabla.Q_t)_{\text{flat}} = \sum_{i=1,\cdots,4} \frac{Q_{t,i}(x,y,t)}{l_{\text{res}}}\, min(\overrightarrow{W_{dir}}.\overrightarrow{n_i}, 0) - \sum_{i=1,\cdots,4} \frac{Q_{t,\text{out}}(x,y,t)}{l_{\text{res}}}\, max(\overrightarrow{W_{dir}}.\overrightarrow{n_i}, 0) \tag{22}$$

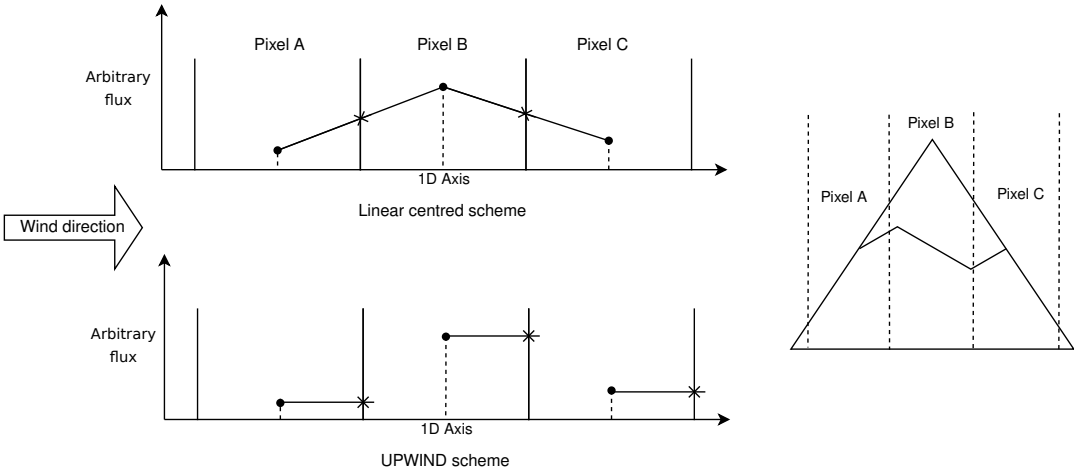

Figure 3. Illustration of the differences between the upwind scheme and a more classic linear scheme for a 1D ideal case. Dots represent the flux estimated for each pixel by Eq 22. Crosses (X) represent the flux value crossing the pixel face. In the linear scheme, the flux value leaving the pixel is the linear interpolation between the two-pixel cell center values. The flux crossing the pixel face can be very different from the cell center computed value. The border flux being linearly interpolated, the border value can be unrealistic. This behaviour can cause interpolation to move erosion out of the expected zone (usually summits, the windiest zone). In the upwind scheme, the flux value crossing the pixel is identical to the cell-centred computed value.

$(\nabla.Q_t)_{\text{flat}}$ was defined in Eq. 20, $min(\overrightarrow{W_{dir}}.\overrightarrow{n_i}, 0)$ and $max(\overrightarrow{W_{dir}}.\overrightarrow{n_i}, 0)$ giving respectively the flux direction coefficient (same as wind direction) crossing each face normally for in and out the direction.

The code implementation of Eq. 22 is explained in more detail in paragraph 3.7.

3.6 Influence of snow transport and deposition on snow surface properties

As, despite a qualitative knowledge of the processes, almost no observation-based parameterization of the influence of snow transport on snow surface properties (Comola et al., 2017; Mott et al., 2018; Amory et al., 2021) is available in the literature, only the following simple considerations were implemented in SnowPappus to represent it:

- Snow deposited by a transport event (when $q_{\text{dep}} > 0$) has the properties of rounded grains with sphericity $s = 1$ and dendricity $d = 0$, and relatively high density $\rho = 250 kgm^{-3}$.
- Wind-induced metamorphism might also originate either from subgrid snow transport or from horizontal displacement of snow with erosion and deposition flux compensating each other. Thus, the preexisting parameterization for wind-induced snow metamorphism from Vionnet et al. (2012) can still be activated, but considering the SnowPappus threshold wind speed instead of the original formulation. It makes the surface snow layers slowly become denser and evolving towards small rounded grains approximately linearly with time. The impact is tested in Sect. 4.3

3.7 Implementation in SURFEX

SnowPappus is implemented inside the SURFEX/ISBA land surface scheme, which computes the evolution of soil and snow properties sequentially. Distributed hardware and needs of communication among grid cells requires the use of the MPI protocol (Clarke et al., 1994), to be able to run distributed simulations over large domains in a short time.

At the beginning of a new simulation, an unpublished domain decomposition already implemented in SURFEX is applied to split the domain in subdomain stripes. The algorithm is designed to balance as much as possible the number of grid cells between the different cores, but all the points with the same zonal coordinate are always gathered on the same core. Therefore, the maximum number of subdomain stripes for an experiment is the number of lines of the domain. Each subdomain is associated with an MPI thread.

For each time step and subdomain, the SnowPappus routine is called before each iteration of the snowpack scheme. It computes the horizontal transport rate, Q_t, and the blowing snow sublimation rate, q_{subl}, for each grid point, according to the surface properties computed in the previous time step. Then, once Q_t and q_{subl} are computed for all pixels, this information is shared with the processors associated with the adjacent grid point by a blocking MPI communication. After this phase, the erosion/deposition rate can be computed with Eq. 22 and converted into an amount of snow to remove or add to the snowpack. If there is net erosion, snow is directly removed in the SnowPappus routine. Otherwise, the falling snow amount and properties are computed in the SnowPappus routine and then given as snowfall input to the Crocus snow scheme.

The Crocus routine is called after SnowPappus. It deals with adding snow to the snowpack and modifying snow layers accordingly to snowfall and SnowPappus outputs. If a snowfall and wind-driven snow deposition occur simultaneously, the amount of added snow is the sum of both. Its density and microstructure variables are a weighted average of falling snow and blowing snow properties. The detailed equations for this process are described in appendix E. The Crocus routine then takes back the original Crocus model course and makes the properties of snow evolve through metamorphism, heat diffusion, compaction, percolation, etc. Those processes are summarized in Fig.4.

It is important to note that transport rate and snowpack evolution are solved in a decoupled mode (one after the other). Therefore, the deposition rate q_{dep} is computed independently from the amount of snow available on the considered grid point, which can make the amount of snow removed from the point to be higher than the available snow mass. In this case, the mass balance is not respected. The cumulative amount of this "ghost snow" is stored in a variable to check it remains small. To prevent this behaviour from occurring, limitations on Q_t and q_{subl} are made. The condition is the following :

$$q_{subl} \leq \frac{W}{t_{step}}$$

$$Q_t \leq (\frac{W}{t_{step}} - q_{subl})\frac{l_{\text{res}}}{cos(\theta)}$$

with W being the snow mass for each pixel in kg m^{-2}, t_{step} the computation time step in s.

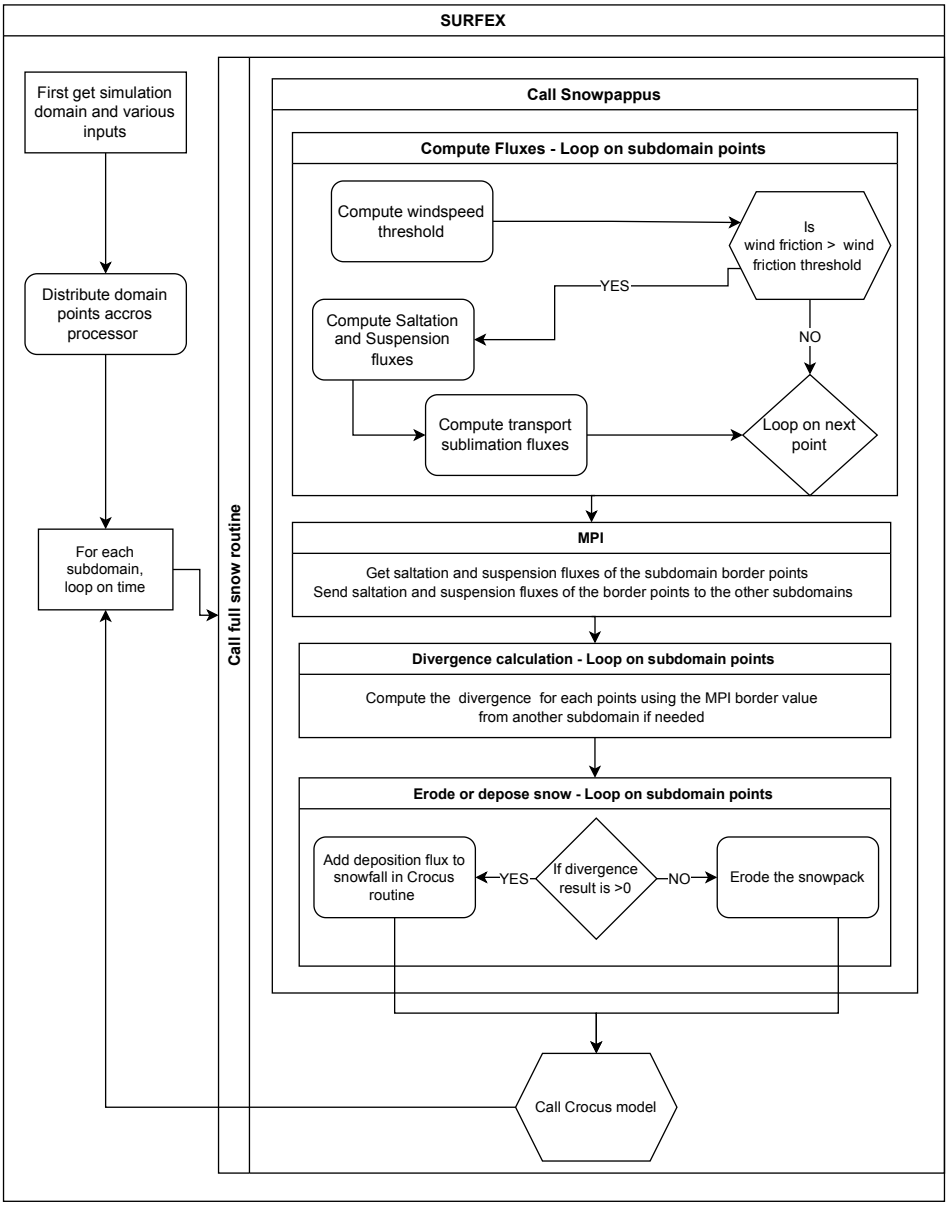

Figure 4. Description of how the SnowPappus routine is organized in the SURFEX framework and how it connects with the Crocus snow model.

4 Evaluation: Methods

4.1 Study area

For demonstration and evaluation purposes, we run simulations over a test zone covering the whole "Grandes Rousses" massif in the French Alps, with a spatial resolution of 250 meters. It covers 14443 grid points (3200 km^2). This area exhibits a complex topography, with elevation ranging from 700 to more than 3500 meters, involving a large range of temperature conditions and snow coverage duration. For this test zone, most winter storms come from North-Western flows. Besides, to demonstrate the ability of SnowPappus to be run over large domains, we also set up a simulation domain containing the whole French Alps with about 868000 simulation points. Both domains are illustrated in Fig. 5

4.2 Meteorological forcing

The Crocus snow model needs various atmospheric forcing variables: liquid and solid precipitations, incoming shortwave and long-wave radiations, air temperature and humidity, wind speed and direction. In this work, all these variables but the wind are given by the SAFRAN reanalysis (Vernay et al., 2022) over geographical units so-called 'massifs' of about 1000km^2 in which meteorological conditions only depend on elevation at a vertical resolution of 300 meters. Here, all meteorological variables are interpolated on a 250 m resolution simulation grid, at the exact elevation of each grid point, derived from a DEM at this resolution (as in Revuelto et al. (2018) and Deschamps-Berger et al. (2022)). The DEM was created by averaging on each grid point the 5 m resolution RGE Alti® DEM, provided by the Institut Geographique National at the scale of France. Snow transport modelling is strongly sensitive to the quality of the wind forcing (Musselman et al., 2015). Consequently wind fields taking into account the effect of local topographic features were preferred to the very large-scale SAFRAN wind fields. Here, km-scale wind fields are first extracted from AROME NWP model at a 1.3 km resolution (Seity et al., 2011; Brousseau et al., 2016), then downscaled at a 30 meters resolution using the DEVINE downscaling method (Le Toumelin et al., 2022) and finally resampled at 250m using a simple average. DEVINE method benefits from the use of convolutional neural networks to downscale winds from AROME to high-resolution local topography, based on preliminary training with wind speeds simulated with ARPS atmospheric model (Xue et al., 2000). Previous evaluations of DEVINE have shown that contrary to basic wind interpolation methods, DEVINE is able to improve wind speed estimations compared to raw NWP model outputs and to reproduce several characteristics of terrain forced flow (speed-up on crests, windward deceleration, channelling through gaps and passes) prone to influence drifting snow episodes.

4.3 Evaluation data

Blowing snow flux data is available for 3 stations in the Grandes Rousses test zone. One of these is the *Col du Lac Blanc* observatory where long-term monitoring of blowing snow fluxes and of various atmospheric forcings have been performed (Guyomarc'h et al., 2019). In particular, a vertical profile of Snow Particle Counters (SPC) (Sato et al., 1993) recording blowing snow fluxes at four different heights, is located at a particularly wind-exposed location. An estimate of vertically integrated

flux between 0.2 and 1.2 m above snow surface is provided from these measurements from 01 December to 01 April since 2010 (Guyomarc'h et al., 2019). The shapes of vertical profile concentration are classified into different categories: 'no flux' when no flux was recorded, 'inconsistent' when flux at the different height was physically inconsistent, 'power-law' when the concentration profile fits with a power-law or 'mean' when the flux depends weakly on height. 'mean' flux is expected when the flux is dominated by solid precipitations, whereas 'power-law' profile is expected when it is dominated by wind-induced snow transport (see Sect. 3.3.1). We use these data to evaluate blowing snow occurrence and fluxes.

The other sites are the Huez (FHUE) and Chambon (FCMB) stations of the ISAW network, which data were already used in blowing snow studies (Vionnet et al., 2018; He and Ohara, 2017). They are equipped with snow height, temperature, wind measurements and Flowcapt sensors (Chritin et al., 1999), which record integrated blowing snow from 0 to 2m above the ground surface. Trouvilliez et al. (2015) indicate that Flowcapt sensors of different generations give similar results with respect to SPC if a threshold value higher than 1 g m^{-2} s^{-1} is taken. However, they can be partially buried under snow depending on snow height and their reliability in terms of estimated flux is still debated in the literature (Cierco et al., 2007; Trouvilliez et al., 2015; Vionnet et al., 2018). Thus, similarly to Vionnet et al. (2018), we use them only to evaluate the blowing snow occurrence. Flowcapt data available in ISAW stations was specifically cleaned up as described in Vionnet et al., paragraph 3.1.

4.4 Model set up

4.4.1 2D simulations

The two-dimensional simulations were performed with the "default" SnowPappus configuration, using the GM98 option for wind speed threshold and deactivating wind-induced snow metamorphism. The simulations were run from 01 August 2018 06:00 UTC to 01 August 2019 06:00 UTC. Soil temperatures were initialized by a model spinup from 01 August 2008 06:00 UTC to 01 August 2018 06:00 UTC in a similar configuration except for the wind which also comes from SAFRAN during the spinup period. This simulation was used for numerical performance assessment and local evaluation of the blowing snow occurrence. A reference simulation where snow transport was deactivated was also run over the same period with the same initial conditions.

4.4.2 Local simulations

The accuracy of wind forcing is known to play a major influence on any evaluation of a snow transport model (Vionnet et al., 2018). Consequently, we also run and evaluate local scale simulations at *Col du Lac Blanc* forced by observed 5-m wind speed in order to distinguish the contributions of wind speed errors and model errors in our results. Wind speed sensors as well as SPC are located on the same mast, at the station "AWS Col" described in Guyomarc'h et al. (2019). Their height above the surface is variable and recorded continuously, allowing to estimate 5-m wind speed assuming a logarithmic wind profile and a roughness length z_0 = 2.3 mm. The other meteorological variables are interpolated from SAFRAN reanalysis as for 2D simulations. In this configuration, blowing snow fluxes are computed by the model but do not result in any erosion or deposition. These local simulations were performed from 01 August 2010 to 01 August 2020 with a soil temperature initialized by a spinup from

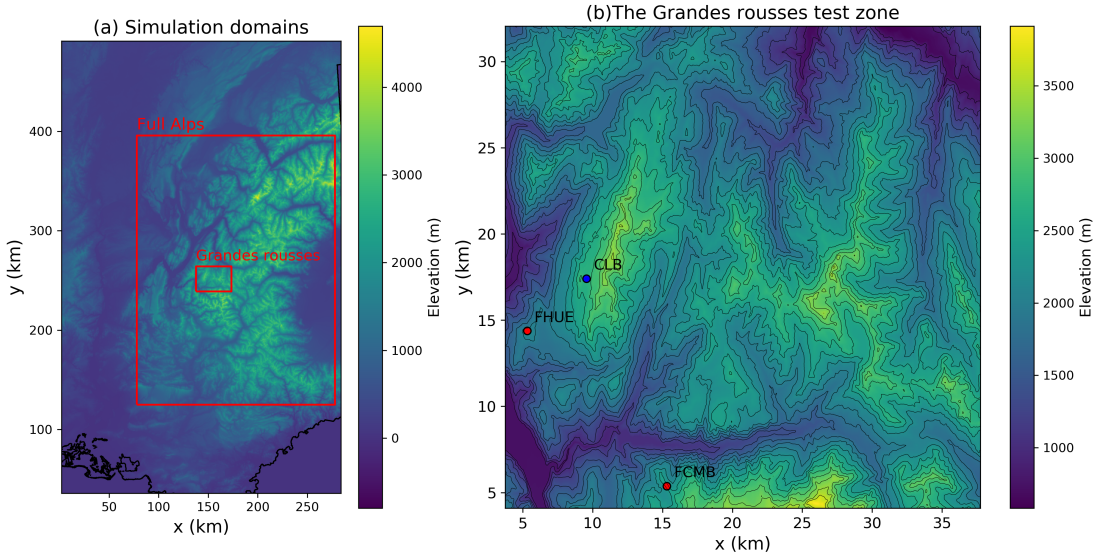

Figure 5. (a) Limits of the two domains used for simulations in the article. The small 'Grandes Rousses' test zone is used for two-dimensional simulations presented in Sect. 5.3. The 'Full Alps' domain was used to test the possibility of running simulations on the entire French Alps (see Sect. 6.5). (b) Topographic map of the 'Grandes Rousses'. The location of the *Col du Lac Blanc* experimental site (blue dot) and of the two flowcapt sensors of ISAW network (red dots) are indicated. Equidistant iso-elevation lines are represented. Data from RGE ALTI® was used to generate these maps.

2000 to 2010. At Col du Lac Blanc, fetch distance in the mean wind direction as defined in Sect. 3.3.2 was estimated to be $110 \pm 20m$, as the mean distance between the SPC sensors and the center of accumulation zones identified from Vionnet (2012, Fig. 4.24). We thus fixed l_{fetch} = 110 m in the blowing snow flux simulations.

Several model configurations were used to investigate the simulated blowing snow occurrence, and are described here:

- **SnowPappus: Run A** SnowPappus default configuration with wind-induced snow metamorphism deactivated (see Sect. 3.6). 'GM98' option is used for threshold wind speed (see Sect. 3.2)
- **SnowPappus: Run B** SnowPappus default configuration with wind-induced snow metamorphism activated.
- **SnowPappus: Run C** SnowPappus with 'CONS' option (see Sect. 3.2), with 5-m threshold wind speed equal to 9 m s^{-1} for snow older than one hour. Note the 9 m s^{-1} was calibrated provide the optimal Heidke Skill Score (see in Sect. 4.5) among different tested values (not shown).
- **Vionnet 2013** SnowPappus with parameters putting it in the exact same configuration as Vionnet et al. (2013) for wind speed threshold calculation and falling snow properties (see Sect. 3.2)

Additionally, to investigate the sensitivity of the simulated fluxes of blowing snow to d_m (Sect. 3.3.1), we tested three modified configurations of run B configuration with d_m values of 0, 0.5 and 1.

4.5 Evaluation of blowing snow occurrence

We evaluate the blowing snow occurrence using the same framework as Vionnet et al. (2018), allowing comparisons with the Sytron operational system, which can be considered as a benchmark. Contrary to SnowPappus, Sytron is based on an 8-aspect idealized geometry (Vionnet et al., 2018). Both systems share the Guyomarc'h and Mérindol (1998) parameterization for threshold wind speed calculation. As Vionnet et al. (2018), we consider blowing snow is *observed* if the blowing snow flux measured by the SPC and integrated between 0.2 and 1.2m exceeded a threshold of 1 g m^{-1} s^{-1} and *simulated* if a non-zero blowing snow flux was simulated, and define blowing snow days as days with more than 4 consecutive hours of blowing snow.

Here, the study was conducted on the whole 2010-2020 period, while Vionnet et al. considered only the 2015-2016 season. As in Vionnet et al. (2018), false alarm rate (FAR), probability of detection (POD) and Heidke skill score (HSS) are used to evaluate the different setups:

$$POD = \frac{a}{a+c} \tag{23}$$

$$FAR = \frac{b}{a+b} \tag{24}$$

$$HSS = \frac{2(ad-bc)}{(a+c)(c+d)+(a+b)(b+d)} \tag{25}$$

with a, b, c, d respectively the number of true positive, false positive, false negative and true negative events. HSS varies between -1 and +1, +1 for a perfect agreement and 0 for a random forecast.

These scores were first applied to the 4 model configurations previously described and to new runs of the Sytron system to cover the same evaluation period and share the same code version of SURFEX-Crocus. For Sytron, as in Vionnet et al. (2018) (although not mentioned in the original publication), the occurrence of blowing snow is considered detected if a non-zero flux is simulated on at least one of the 8 slope aspects.

The occurrence scores are then applied to the 2D simulation outputs for the 2018-2019 season, driven by simulated wind fields as described in Sect. 4.1. The evaluation is carried out at *Col du Lac Blanc* station and at both ISAW stations. Each station was associated with the closest grid point from its location.

4.6 Evaluation of blowing snow fluxes

Integrated blowing snow fluxes between $z_{min} = 0.2m$ and $z_{max} = 1.2m$, called $Q_{t,int}$ were evaluated against SPC data. Modelled flux is computed at each time step as :

$$Q_{t,int} = \int_{z_{min}}^{z_{max}} q_{\text{susp}}(z)dz = \frac{c_r z_r u_*}{k(1-\gamma)}[(\frac{z_{max}}{z_r})^{-\gamma+1}(\log(\frac{z_{max}}{z_0}) - \frac{1}{1-\gamma}) - (\frac{z_{min}}{z_r})^{-\gamma+1}(\log(\frac{z_{min}}{z_0}) - \frac{1}{1-\gamma})] \tag{26}$$

Note that the blowing snow flux below 20 cm in height cannot be accounted for in this evaluation, although it may represent a significant contribution to the total flux. Observed data are available with a 10-minute time step. For evaluation purposes,

model output and SPC fluxes were first averaged hourly. As the observed fluxes cannot be used when precipitating particles prevail, periods when at least one 'mean' concentration profile was observed were removed. Considering the other missing data, 4947 hours of data are considered in the evaluation.

To assess the ability of SnowPappus to capture the long-term magnitude of wind-induced snow transport, monthly averages of simulated fluxes were compared to the observed ones, keeping only the months when at least 15 days of valid observed data are available. Hourly data were also classified distinguishing two cases : (i) days with snowfall according to SAFRAN reanalysis and (ii) days with no snowfall. Observation-derived wind friction velocity was also classified in 20 equally distant wind speed intervals (interval widths are about 0.064 ms^{-1}). Averaged observed and modelled flux by category and wind speed step were computed and compared. Less than 20 hours of data were available by wind steps for $u_* > 0.95\ ms^{-1}$ so these wind speeds were not considered.

These scores were applied to the 3 variants of Run B configuration (3 values of d_m).

5 Results

5.1 Comparison of saltation parameterizations

We now compare the outputs of **S04** and **SnowPappus+P90** methods (see Sect. 2.2.4), which compute the blowing snow flux up to h_{susp} = 10-15 cm. The results of the method **SnowPappus+P90** depend on the value of h_{susp}. Thus, we computed the blowing snow flux with this method between 0 and 10 cm (height of Nishimura and Hunt experiment) and between 0 and 15 cm (height used by Melo et al. to compare S04 with their more complex saltation model). Results are presented in Fig. 6 and shows that the predicted fluxes by both models give close results for friction velocities lower than 0.6 m s^{-1}. We conclude that the huge difference observed between S04 and P90 is resolved at low wind speed by adequately representing the bottom of the suspension layer which is implicitly included in the S04 formulation. Both formulations give there a flux of the same order of magnitude and thus experimental and theoretical validations of S04 are also in agreement with SnowPappus. At high wind speed, both formulations diverge (around 0.6-0.7 m s^{-1} for h_{susp} = 10 cm, 0.8-0.9 m s^{-1} for 0-15 cm), with P90+SnowPappus fluxes tending to curb down. This behaviour is clearly due to the fast growth of h^{P92} with wind speed, making the low P90 saltation flux applied to most of the 0 - 15 cm layer. It must be noted that observations and simulations used for validation of the formulations are in the range 0.2 - 0.85 m s^{-1} (Pomeroy and Gray, 1990; Pomeroy and Male, 1992; Nishimura and Hunt, 2000; Melo et al., 2022). Hence, both formulations might give unreasonable results at higher wind speeds. Thus, we argue both P90 and S04 give consistent results compared with other parameterizations of the literature for low to moderate wind speed.

By default, we choose to use the P90+SnowPappus option in SnowPappus, as it gives a more coherent link between saltation and suspension, and because of better empirical support of P90.

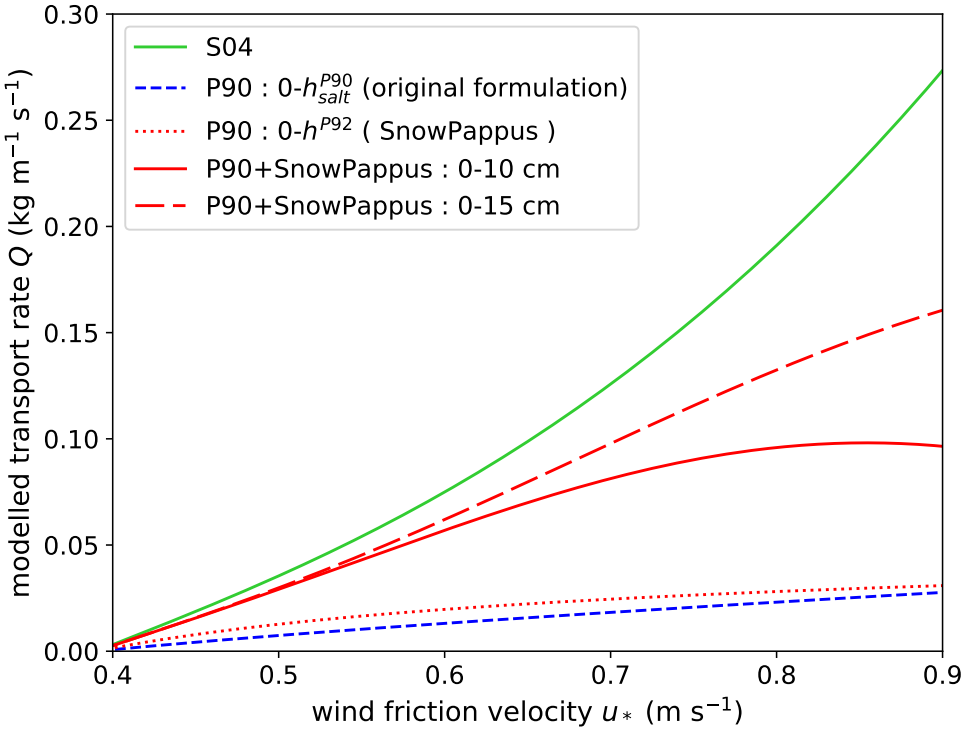

Figure 6. Comparison of the predicted flux in the saltation layer and the transition with suspension (up to 10 - 15 cm) with the two methods described in Sect. 2.2.5 based on P90 (blue curve) and S04 (green curve). P90-modelled flux is computed up to (i) the integration height h^{P92}, which corresponds to the entire "saltation" layer, (ii) 10 cm which is the height on which are integrated Nishimura and Hunt measurements used to calibrate S04 parameterization and (iii) 15 cm which is the height used by Melo et al. to compare S04 with a more complex saltation model, with good agreement shown (red curves). Here, all the modelled fluxes are computed for a threshold wind speed $u_{*t} = 0.39ms^{-1}$, and the type of snow used in SnowPappus is old (non-dendritic)

5.2 Comparison of simulated blowing snow flux with simple parameterizations in the literature

Before evaluating SnowPappus against observations, the relationship between Q_t and wind speed is illustrated in Fig. 7 for fresh and old snow, and compared to other estimates from the literature. It stresses that, due to a lower terminal fall speed of snow particles, fresh snow exhibits much higher transport rates than old snow. The model of Essery et al. (1999) exhibits results almost identical to the "old snow" case of SnowPappus. Compared with empirical observations of Mann et al., SnowPappus transport rates simulated in both cases are in the range of the very spread observed values, at least for wind speeds lower than 20 m s^{-1}. The fresh snow case seems to correspond approximately to the upper bound of observations. These observations show that at least the magnitude of SnowPappus flux is plausible.

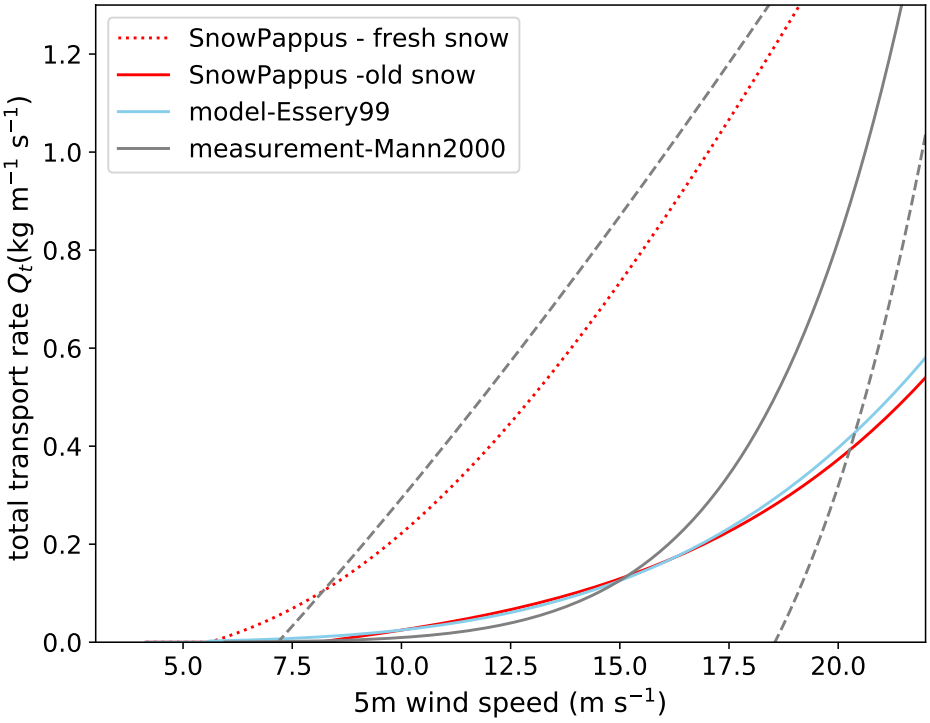

Figure 7. Total blowing snow flux Q_t predicted by SnowPappus as a function of 5-m wind speed, for old and fresh snow (red lines, see Fig. 2 for old and fresh snow discrimination). The blue line represents the flux predicted by a simplified theoretical model (Essery et al., 1999), assuming $z_0 = 1mm$ and the grey line represents an empirical formula derived from observations in Antarctica (Mann et al., 2000) $Q = 1.504u_*^5.144$ and taking $z_0 = 5.6.10^{-5}m(\frac{u_*}{0.3ms^{-1}})^2$ as the authors of the studies. The dashed grey lines represent the upper and lower bounds of the observed flux, roughly estimated from Fig. 6 of the article.

5.3 Illustration of simulation output over Grandes Rousses study area

Synthetic simulation outputs of the simulation performed during the whole 2018-2019 winter season are presented in Fig. 8. The cumulated erosion/deposition rate during the whole season is low over a large part of the domain but it reaches absolute values of around 500 kg m^{-2}, which are comparable to the total amount of solid precipitation in the area, in some points. As expected, hot spots of transport are located around high alpine crests, generally limited to the crest summit and the two adjacent grid cells. Higher deposition seems to usually occur on the Eastern side of the crest, consistently with the prevailing winter storms coming from North-Westerly Atlantic flows.

The relative average snow depth change compared to the simulation where snow transport was deactivated is also shown in Fig. 8. It is very similar to the deposition pattern, and also shows that some crests summits experience almost complete snow

removal due to transport (relative change close to -1) whereas the amount of snow is more than doubled in some deposition zones.

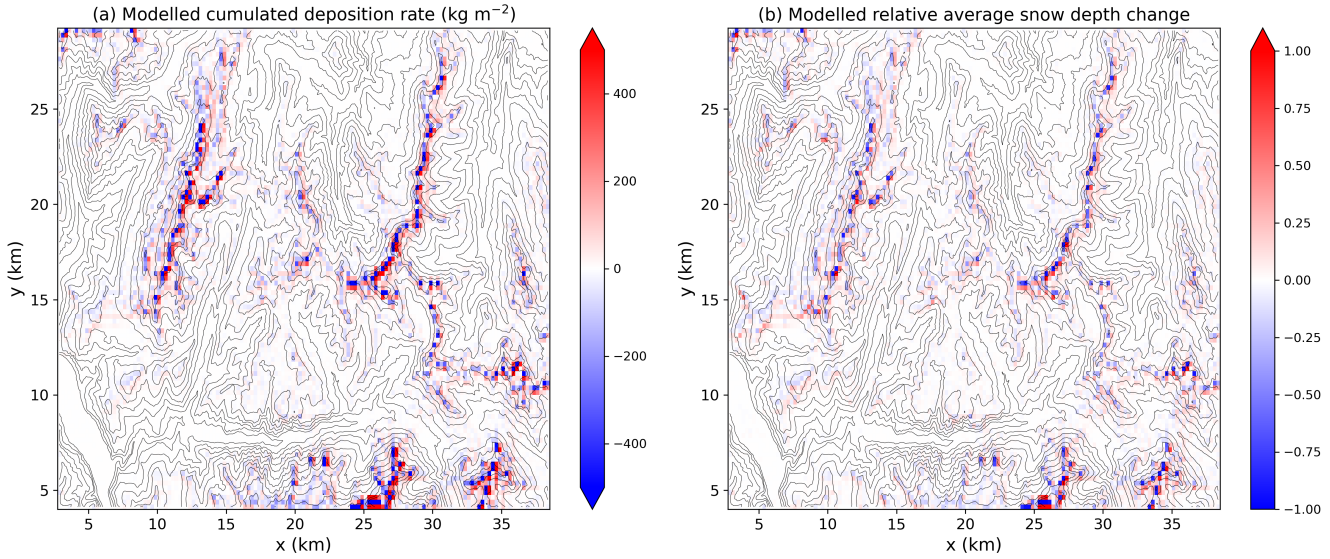

Figure 8. (a) Cumulated deposition rate $\sum_{t_i} q_{\text{dep}}(t_i)$ simulated by SnowPappus transport scheme during the whole 2018-2019 winter season in the whole Grandes Rousses test zone.**(b)** Relative difference in yearly-averaged snow depth h_s between a simulation with transport (w.t.) activated and simulation without transport (n.t.) $\Delta h_s = \frac{h_s^{w.t.} - h_s^{n.t.}}{h_s^{n.t.}}$

5.4 Evaluation of blowing snow occurrence at Col du Lac Blanc

HSS, FAR and POD of the different setups are compared on Fig. 9 for all days and for the days without snowfall. Probabilities of detection range typically from 80 to 90 %, and false alarm rates from 30 to 40 % considering the whole period. FAR are higher (40-60 %) considering only days without snowfall.

The SnowPappus default option (run A) exhibits slightly lower FAR and POD than the approach of Vionnet et al. (2013) (run D), which leads to similar HSS, in particular when considering only days without snowfall. Accounting for wind-induced snow metamorphism option (run B) modifies only slightly the scores and did not improve the detection of blowing occurrence. All these methods including a threshold wind speed that depends on the properties of surface snow exhibit high false alarm rates, and do not perform better than using a constant 5-m threshold wind speed in no-snowfall conditions (run C). In addition, SnowPappus, with its different options, and Sytron operational model exhibit similar scores.

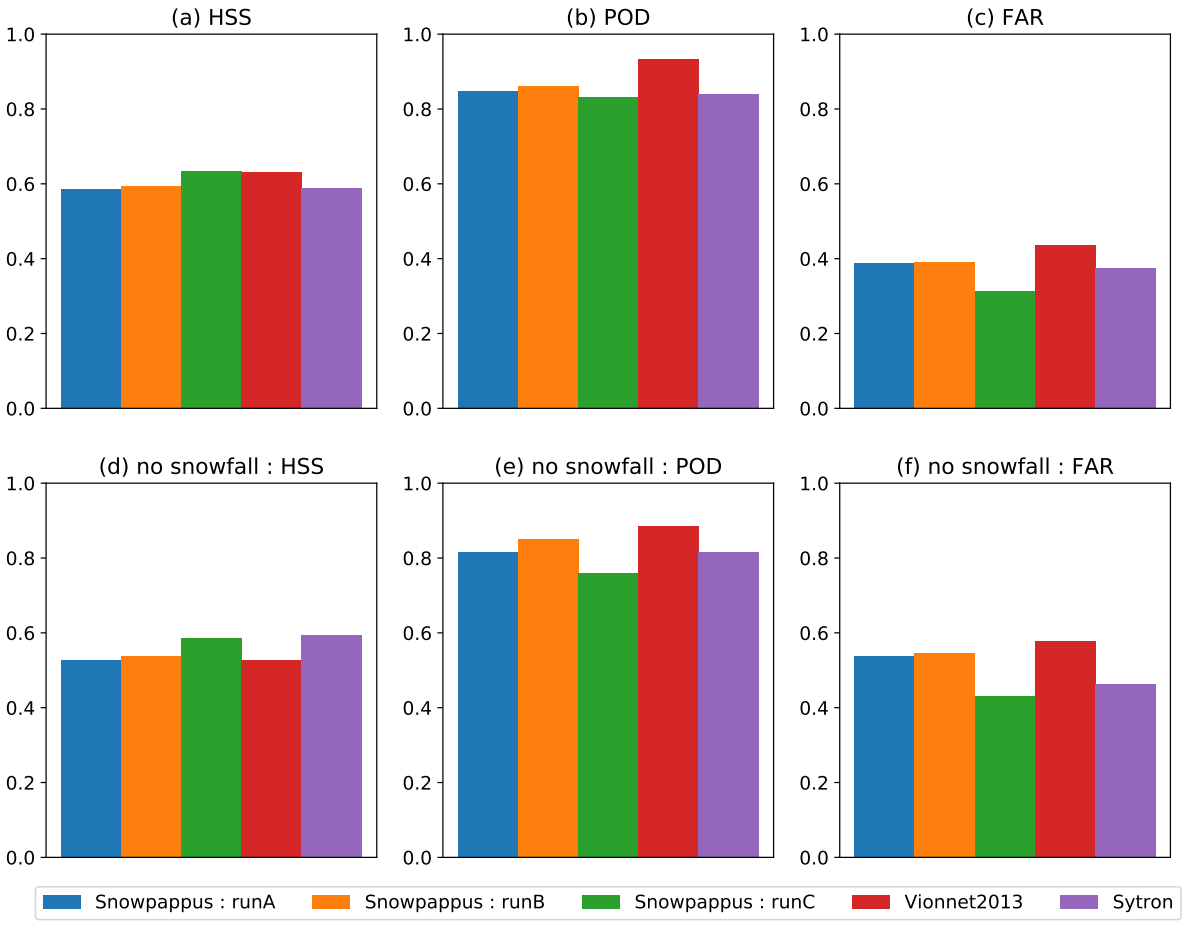

Figure 9. Evaluation of the detection of blowing snow days with point-scale SnowPappus simulations and Sytron operational system. HSS (a,d), POD (b,e) and FAR (c,f) of different SnowPappus configuration and other models, computed from all days independently (a,b,c) and only for days with no snowfall(d,e,f) are represented. As more detailed in Sect. 4.5 ,Run A is default SnowPappus configuration, run B is the same with wind-induced snow metamorphism, run C uses a constant threshold wind speed for dry snow older than 1 hour and 'Vionnet2013' is supposed to reproduce the configuration described in Vionnet et al. (2013).

5.5 Evaluation of blowing snow occurrence in 2D simulations

Scores of blowing snow detection obtained with 2D simulations at *Col du Lac Blanc*, Huez and Chambon stations are shown in Fig. 10. HSS and POD are low in this configuration using wind speed downscaled at 250-m grid spacing using the DEVINE approach. At Col du Lac Blanc, the HSS is lower than the HSS obtained for point-scale simulation forced by observed wind speed. This decrease in HSS mainly results from a strong decrease in POD (Fig. 10b). It suggests that the accuracy of downscaled

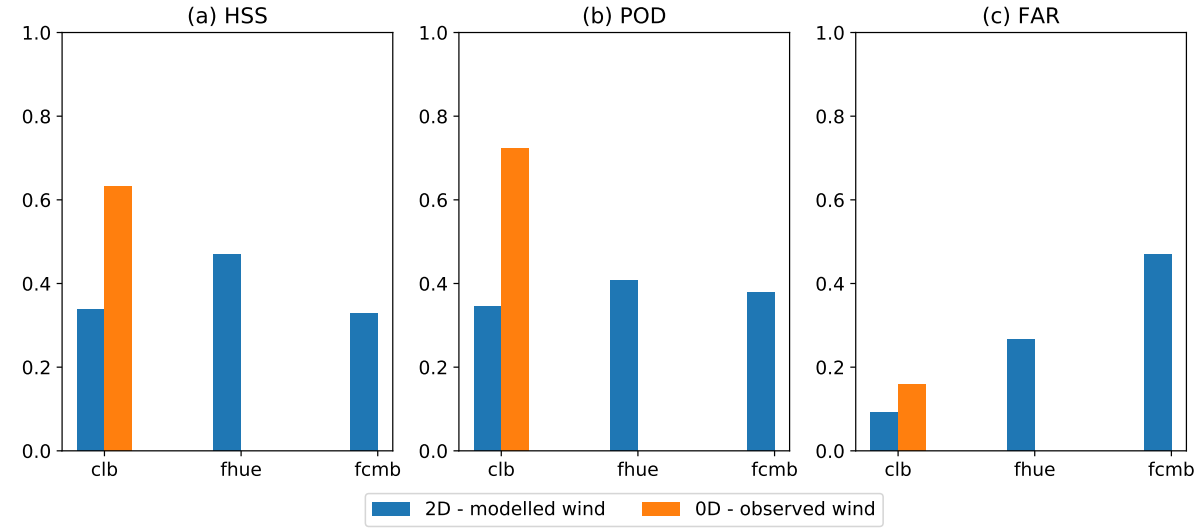

Figure 10. Blue bars: HSS, POD and FAR for the detection of blowing snow days in 250 m resolution simulations against Flowcapt data of ISAW stations of Huez (fhue) and Chambon (fcmb), and SPC data from *Col du Lac Blanc* (clb). Orange bars: same scores in point-scale simulations with the same SnowPappus configuration forced by observed wind speed (Run A in Fig. 9)

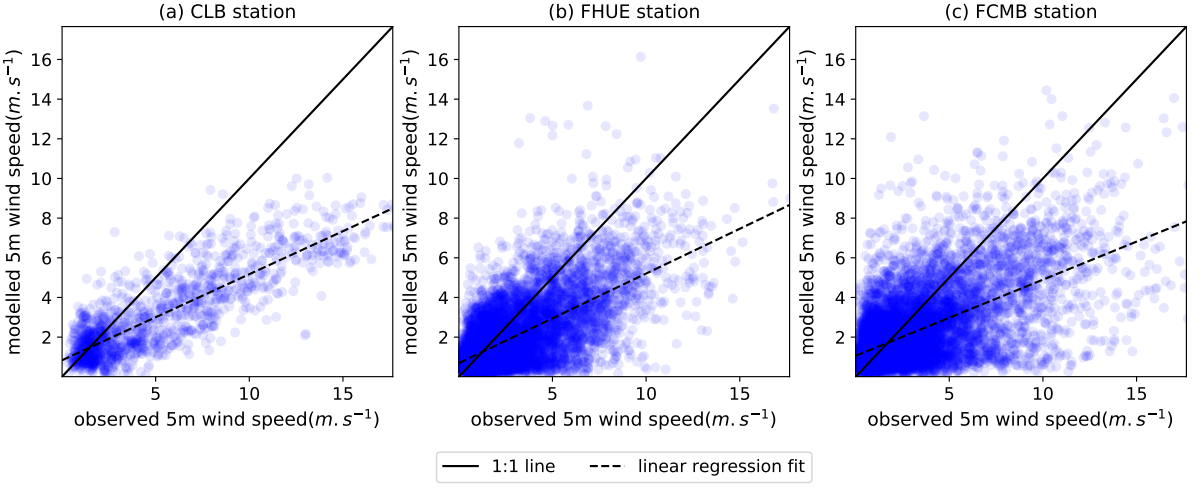

Figure 11. Comparison between observed wind at *Col du Lac Blanc* and at Huez and Chambon ISAW station and the 250m resolution DEVINE-modelled wind used as a forcing in the closest simulation points. Linear regression line fitting the modelled wind as a function of the observed ones are presented. The presented points are the ones used for blowing snow occurrence evaluation in Fig. 10. Wind observed data were filtered using the same algorithm as Le Toumelin et al. (2022)

wind speed and/or the 250 m spatial resolution of the simulation are the main causes of the skill deterioration, as confirmed by the significant discrepancies between observed and simulated wind speeds at the three stations (Fig. 11). A negative bias in simulated wind speeds is observed, in particular for strong winds, explaining the low detection rates.

5.6 Evaluation of blowing snow fluxes at Col du Lac Blanc

Figure 12a shows the simulated monthly averaged fluxes between 0.2 and 1.2 m $Q_{t,int}$ at *Col du Lac Blanc* as a function of the observed ones, for the 3 tested d_m values. As expected, fluxes clearly increase when d_m decrease, because it makes the terminal fall speed closer to the fresh snow regime. Simulated $Q_{t,int}$ is of the same order of magnitude as the observed one. It is clearly overestimated when $d_m = 0$ case, clearly underestimated when $d_m = 1$ and slightly underestimated when $d_m = 0.5$. In all cases, modelled fluxes seem to correlate well with observed ones, however with a strong dispersion. In particular, one specific month has a simulated flux 8 times higher than the observed one regardless of the d_m value, and will be discussed in Sect. 6.1.

Figure 12b shows average simulated and observed fluxes as a function of the 5m-wind velocity u_* for days with and without snowfall, for wind friction velocities between 0 and 0.95 m s^{-1}. Simulated and observed fluxes show the same dependency with u_*, the flux remaining negligible under a threshold wind speed and then increasing in a steady non-linear way. Moreover, both observed and simulated fluxes are higher during days with snowfall than during days without snowfall. Therefore, we can state that SnowPappus reproduces correctly the dependency of blowing snow flux on snow age and wind speed. In particular, the relationship between $Q_{t,int}$ and wind speed is very close to the observed one in the case of $d_m = 0.5$.

5.7 Numerical performance

In this section, we describe the numerical performance of the SnowPappus model to discuss its suitability for the goal of applicability in large-scale systems operated at hectometre resolution.

Computation time was measured for the simulation domain covering the Grandes Rousses range (Sect. 4.1). Computations are done using one node of the current Meteo-France supercomputer made of 2 AMD Rome 2,2 Ghz CPU giving a total 128 computing cores and 256 Gb node RAM. For the Grandes Rousses domain, the maximum possible number of threads is 101 (see Sect. 3.6) To time the execution of different parts of the code on a distributed set of cores, we use the DrHook profiling tool(Saarinen et al., 2005). To obtain the user run time of non-overlapping and blocking code sections, we sum the maximum computing thread time for each code section.

Figure 13 shows the maximum thread execution time for each code section of the SnowPappus blowing snow model and compares these durations to the full snow routine of SURFEX which contains mainly the SnowPappus routine and the Crocus snow model, for different degrees of parallelisation. Its execution time decreases sharply with the number of threads used, however reaching a plateau at 60 cores and above. Almost all of the SnowPappus computing time is dedicated to MPI communications. Therefore, the proportion of time spent in SnowPappus routine grows with the number of threads used, becoming eventually more time-consuming than Crocus (it is shown more visually into appendix Fig. A2) , indicating it benefits less than Crocus from increased parallelization. It can be explained by the increased number of MPI blocking communications. Indeed

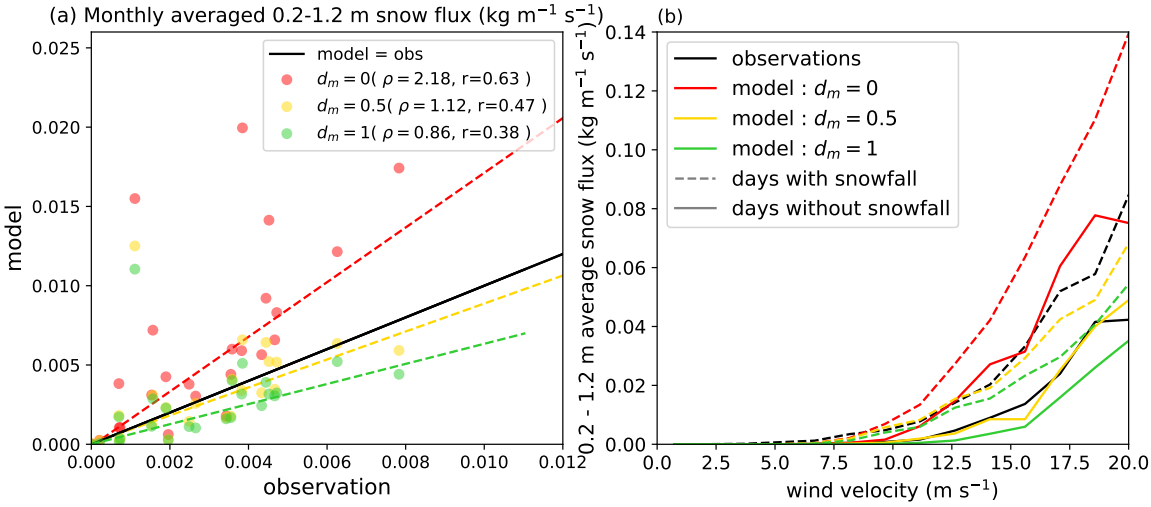

Figure 12. **(a)** Simulated monthly-averaged $Q_{t,int}$ at *Col du Lac Blanc* as a function of SPC-observed fluxes, for 3 different values of d_m. The 1:1 line representing equality between the model and observations is drawn in black. The dashed lines are Theil Sen regression fits (Wilcox, 1998) of each model configuration. Ratio model-observation of total cumulated fluxes (ρ) and correlation coefficient (r) are indicated in the legend. **(b)** Observed and modelled $Q_{t,int}$ (with the same model configuration as (a)) averaged by 5m-wind velocity intervals, as a function of the interval mean wind friction velocity. Dashed lines are computed from the data for days with snowfall and plain lines with the data for days without snowfall.

communication time and waiting time between thread should grow with the number of subdomains as the workload cannot be equally shared among them.

6 Discussion

6.1 Quality of point-scale flux prediction and comparison with other studies

We evaluated SnowPappus in terms of blowing snow occurrence against point-scale measurements. We also evaluated the simulated fluxes against observed fluxes in a part of the suspension layer. As model outputs are highly dependent on wind speed (Fig. 7), we first discuss the model skill of point-scale simulations at *Col du Lac Blanc* forced by observed wind speeds.

Blowing snow occurrence detection in SnowPappus and Sytron operational system (Vionnet et al., 2018) are based on formulations derived from Vionnet et al. (2013) algorithm (hereafter VI13). We performed a long-term evaluation of this process within SnowPappus, VI13 and Sytron at *Col du Lac Blanc* observatory on the 2010-2020 period. It can be compared to other evaluations of VI13 and Sytron systems performed on the same site respectively on the 2001-2011 and 2015-2016 periods (Vionnet et al., 2013, 2018), especially since we intended to reproduce at best Vionnet et al. (2018) methods. Our results show VI13, SnowPappus and Sytron exhibited similar scores, and are interestingly coherent with the previous evaluation of VI13

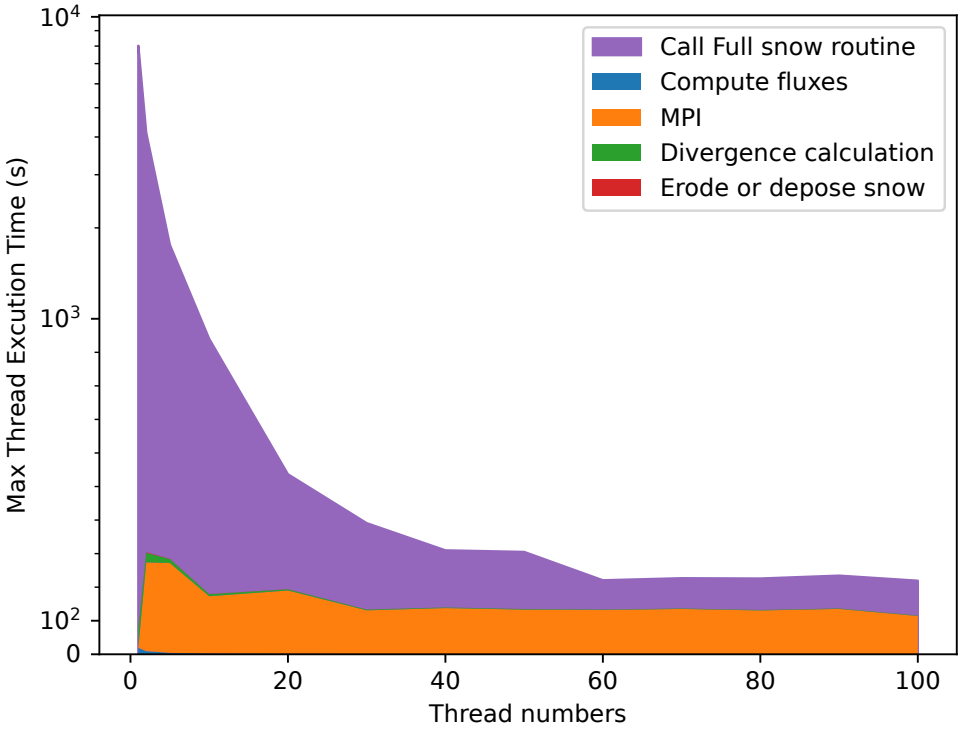

Figure 13. Visualisation of the maximum thread execution time spent in the different parts of SnowPappus (named as in Fig. 4) and spent in the others snow routines. This time is mainly dedicated to run Crocus snow model.

on a different period. All three methods give reasonable but perfectible detection scores with a large false alarm rate, even if (Vionnet et al., 2013) argued in a similar context that it may mainly concerns events with very low simulated blowing snow fluxes. However, the previous evaluation of Sytron by Vionnet et al. (2018) showed better performances, with a perfect detection of blowing snow events on a daily time scale at *Col du Lac Blanc* for one winter, which differs notably with our own Sytron evaluation. We were able to retrieve the original simulation outputs of Vionnet et al. (2018) and applied our evaluation process to these data (see *code availability*), obtaining results very close from ours. Thus, after discussion with the authors, it is clear that the issue comes from unreproducible data post-processing applied to the SPC data to compile results at the daily time scale.

In terms of fluxes, evaluation of the monthly averaged blowing snow fluxes integrated between 0.2 and 1.2 m was performed with different parameterizations of the effective terminal fall speed v_f^*. It shows SnowPappus is able to simulate satisfactory average fluxes at *Col du Lac Blanc* if v_f^* is adequately calibrated. However, simulated fluxes suffer from a high standard deviation of the error, leading to a low correlation between observed and simulated data. A particular outsider monthly value

can be identified in Fig. 12, but, given the meteorological condition during the associated month (see the appendix Fig. A3), it probably comes from a detector failure rather than from a model overestimation. Moreover, Fig. 12a shows the flux dependency on wind speed and snow age is correctly reproduced by SnowPappus. Overall, this point-scale evaluation of snow fluxes at *Col du Lac Blanc* shows SnowPappus provides good orders of magnitude of blowing snow suspension fluxes and occurrence when an observed wind forcing is used. However, the model exhibits a strong uncertainty at the event time scale.

A major strength of our evaluation is the long-term period encompassing 10 winter seasons while most previous studies evaluating simulated blowing snow fluxes in seasonal snowpack conditions only considered a few blowing snow events taken within a period of time of typically one month (Pomeroy and Male, 1992; Naaim-Bouvet et al., 2010; Vionnet et al., 2014). Considering the dispersion of the monthly averaged fluxes we obtain, such short evaluations may be strongly biased. In particular, Naaim-Bouvet et al. (2010) evaluated a formulation of blowing snow flux which is very close to ours in the case of fresh snow but assuming an infinite fetch. Contrary to us, their model overestimated the flux by an order of magnitude, which could be due to the combined effect of the infinite fetch assumption and the specificity of the two considered events. Longer-term evaluations of blowing snow fluxes could be found in Antarctica. For example, an evaluation of the monthly averaged flux simulated by the MAR model in Antarctica was performed at 2 stations with respectively 2 and 8 years time series (Amory et al., 2021). Correlation coefficients of 0.6 and 0.8 were obtained between observation and model. The correlation we obtain is close or inferior to their results for the first station, although the results are not fully comparable (different seasonality of the fluxes, use of simulated wind speed, etc.). Qualitatively, all the mentioned studies obtained a strong dispersion of model errors which is consistent with our results.

However, The use of Flowcapt and SPC data during precipitation events for evaluation purposes is questionable. Indeed, some field evaluations suggest the less rounded snow particle shape in these conditions leads to bias of the flux estimates (Sato et al., 2005; Trouvilliez et al., 2015). Moreover, both instruments do not distinguish blowing snow particles from precipitating snowflakes, which by themselves can be responsible for fluxes of typically 0.1 to 10 g m^{-2} s^{-1} (Vionnet (2012), Fig. 4.17b, Vionnet et al. (2017), Fig. 7). This may deteriorate our results for blowing snow occurrence, as we did not take this possibility into account.

6.2 Sensitivity, added value and robustness of microstructure-dependent parameterizations

We performed blowing snow suspension fluxes evaluation making the parameter d_m, which influences the terminal fall speed, vary within a range which is compatible with the current state of knowledge. Results show that (i) the value $d_m = 0.5$ allows for simulations of realistic average fluxes and (ii) the value of the flux is strongly influenced by d_m, which can make its cumulative value vary by almost a factor 3 in the explored range. d_m controls the terminal fall speed of suspended particles, so it highlights the extreme sensitivity of suspension to this parameter, which is for now imprecisely known.

On the other hand, results on the blowing snow occurrence at *Col du Lac Blanc* suggest that the differences between VI13 method and SnowPappus do not lead to significant differences in the quality of the simulations. Consequently, in the current state of knowledge, both methods can be used. Results also show that the wind-induced snow metamorphism option seems to have only a very small effect on the simulated blowing snow occurrence. It means it might not enhance the quality of

simulation in the alpine environment, although complementary evaluations of its impact on the snow stratigraphy would be required, in particular within 2D configurations of the model. Moreover, for the first time to our knowledge, we compared the results of these parameterizations based on microstructure to a much simpler one where the wind speed threshold depends only on whether or not snow was deposited less than 1 hour ago. It emphasizes that a well-calibrated constant threshold wind speed performs as well or even slightly better than those parameterizations.

However, considering some limits in our study, the above statements must be taken with caution. Indeed, only blowing snow fluxes integrated between 0.2 to 1.2 m were evaluated, which ignores what happens in the saltation layer and in the saltation-suspension interface. Moreover, evaluations and calibrations on flux and occurrence were applied to only one site, with particular climate and environmental conditions. The calibrations of d_m and of the constant threshold wind speed may be over-calibrated to this site and thus not directly valid or optimal at other sites. The absence of added value of Guyomarc'h and Mérindol (1998) at *Col du Lac Blanc* may indicate that it does not captures the temporal variability of threshold wind speed at this site, or that simulated snow surface properties are not relevant.

6.3 Main limitations and improvement opportunities

SnowPappus model outputs depend on two major steps which are (i) computing the local blowing snow fluxes and (ii) computing snow redistribution among grid points. Both steps are subject to large uncertainties which limit the accuracy of the final snow cover simulations. In this section, we discuss the main sources of uncertainties. Snow redistribution in 2D simulations has not been evaluated in this article, due to several methodological challenges including dealing with the superposition of errors coming from the precipitation fields and finding relevant metrics. It will be the subject of a future study expected to provide complementary insights to the following discussions.

6.3.1 Uncertainty on parameterizations

Local fluxes evaluation results suggest the complexity of parameterizations, at least for suspension fluxes and blowing snow occurrence, is not directly linked with model accuracy. Indeed, our simple suspension model exhibited a very high sensitivity to the snow particle effective terminal fall speed v_f^*, which is also involved in more complex suspension models (Bintanja, 2000; Vionnet et al., 2014). Thus, enhancing our knowledge of this parameter and its link to snow properties may allow a larger improvement of suspension flux simulation than complexifying the models. Besides, simplification of the threshold wind speed dependency on snow properties, as well as the inclusion of wind-induced snow metamorphism, did not change significantly the blowing snow occurrence prediction skill. It could be explained by the fact that the interest in such parameterizations can also be limited by intrinsic errors of the Crocus model in terms of surface properties. The hypothesis that a unique threshold wind speed can be used for initiation and stop of the transport in given conditions may also affect this conclusion, as well as the time step of the model which is longer than the duration of individual continuous transport events (Doorschot et al., 2004). Consistently with our results, it must be noticed that recent development in MAR by Amory et al. (2021), including among others a simplification of the threshold wind speed parameterization, led to an improvement of the model skill.

Finally, there are many "blind points" of the snow transport literature that limit the possibility to parameterize some phenomena which may have a strong influence. For example, we could not find any study about the influence of the slope on snow saltation transport, whereas it was shown to influence sand transport (White and Tsoar, 1998) and steep slopes are common in complex terrain. Besides, a large part of wind-induced snow transport events occurs during snowfall (Vionnet et al., 2013). However, saltation fluxes and initiation were never studied during snowfall events to the best of our knowledge, whereas snowfall obviously changes snow cohesion, properties and interacts with grain ejection mechanisms. Finally, quantitative information about the action of transport on snow surface properties still lacks, despite some recent results on density evolution (Sommer et al., 2018; Amory et al., 2021). We think field or wind-tunnel measurements of snow SSA and density in snow deposition zones, as well as observation of their temporal evolution during blowing snow events, would maybe allow to test and improve the hypothesis we had to do for SnowPappus development.

6.3.2 Wind forcing

Simulated blowing snow fluxes increase quickly and not linearly with wind speed as shown in Fig. 7, and pointed out previously by numerous authors (Essery et al., 1999; Mann et al., 2000; Schneiderbauer and Prokop, 2011b, ,...) which found transport fluxes to be approximately proportional to power 4 to 5 of u_*. It consequently makes predicted blowing snow fluxes highly sensitive to the quality of the wind forcing. In addition, poor results for blowing snow occurrence were obtained using 2-dimensional outputs forced by DEVINE modelled wind speed, which is partly explained by the important difference between the value of this wind taken at the closest grid point and the local one. These results suggest the quality of the local wind forcing can easily become a major limiting factor for local blowing snow fluxes assessment. Moreover, it may become even more limiting for the prediction of the spatial erosion and deposition patterns (Musselman et al., 2015). The improvement of wind fields assessment in mountainous areas is beyond the scope of this study but has recently been investigated by several authors (Raderschall et al., 2008; Helbig et al., 2017; Dujardin and Lehning, 2022). Therefore, the possibilities of improvements in snow transport modelling depend heavily on the incoming advances in this area.

6.3.3 Spatial resolution

On the one hand, two-dimensional simulations on the Grandes Rousses test zone (see Sect. 5.3) showed that activating snow transport can have a very strong effect on snow accumulation in the most exposed zones. These effects can be of the same order of magnitude as the amount of annual precipitations in the region (1532 mm of precipitations recorded from 01 August 2018 to 01 August 2019 at the automatic weather station of Alpe d'Huez, coordinates 45.087833°N, 6.085667°E). It suggests that neglecting wind-induced snow transport at this scale is irrelevant for high alpine crests. On the other hand, the width of areas strongly influenced by transport encompasses typically a few grid points. Thus, we can expect results to be hampered by strong numerical errors and discretization issues, as suggested by previous studies at 25-200 m resolution (Lehning et al., 2008; Bernhardt et al., 2009; Grünewald et al., 2010). It highlights also the difficulty of carrying local evaluation of a distributed model at such resolution in complex terrain, as gridded meteorological forcings, in particular wind, and consequently simulated

snow conditions do not necessarily correspond to local ones. Further evaluations of SnowPappus using distributed observations from remote sensing (snow depth, snow cover) will provide further insights into this discussion.

6.4 Limits of applicability

SnowPappus development relied mostly on parameterizations inferred from observations averaged on a 7.5 - 10 min period and performed in environments with seasonal snowpack and at mid-latitudes (Pomeroy and Gray, 1990; Pomeroy and Male, 1992; Vionnet et al., 2012) which is corresponds approximately to our goals in terms of time step and environment for our model applications. Use of these parameterization at much smaller time steps or in very different snow conditions may result in bias. In the case of time step, these concerns are due to the fluctuating nature of wind and non-linear dependence of blowing snow-related quantities on it. Besides, moving to much higher resolutions than 250 m or simpler topographies would possibly require a better treatment of non-local effects by taking explicitly fetch distance into account and solving a 3D advection-diffusion equation.

6.5 Applicability at large scale

The technical possibility to apply SnowPappus in large-scale simulation was one of the targets of this work. The detailed evaluation of its computing performance provided in Sect. 5.7 shows that computing time of SnowPappus physical routine is negligible compared with the one of Crocus. However, scalability issues caused by MPI communications in a highly parallel environment are an important limitation. Reducing the number of communications and homogenizing the workload among threads would alleviate this issue. To achieve it, optimal sub-domain cutting could use squares instead of stripes or even take advantage of snow cover duration (SCD) climatology, as the numerical cost of Crocus-SnowPappus increases strongly with SCD. Despite these current limitations, we were able to perform a yearly simulation on a domain covering the full French Alps (see Fig. 5) in 17h of simulation time using only one computing node. It means daily operational simulations implying 8 days of simulations in the current French system (Morin et al., 2020b) would require only 30 min computing time on one node, which is affordable. Therefore, the main criteria for using SnowPappus in an operational system in the near future will be our ability to demonstrate its added value on the snow cover simulations rather than computation time limitations.

7 Conclusions

This paper presents SnowPappus, a new blowing snow model coupled with the Crocus state-of-the-art snow scheme. It aims to be part of a future operational system running distributed snowpack simulations over the entire French mountains at 250-m grid spacing. SnowPappus is a simple model computing blowing snow fluxes using semi-empirical parameterizations to represent saltation and solving suspension in a one-dimensional stationary state, as models like PBSM (Pomeroy et al., 1993) or SnowTran3D (Liston and Sturm, 1998). It includes newer results on the terminal fall speed of snow particles (Naaim-Bouvet et al., 2010; Vionnet, 2012) which have a strong influence on the simulated snow fluxes, and a parameterization of the threshold wind speed based on Crocus-simulated microstructure properties. Several options are available to represent threshold

wind speed, suspension, sublimation and wind-induced snow metamorphism. MPI parallelization handles the data sharing between neighbouring points required to compute snow redistribution on parallel computers. Performance tests show that Crocus coupled with SnowPappus is able to run a simulation over the full French alps during an entire snow season within a reasonable computation time. However, MPI communications and waiting times raise significantly the computation time.

Local evaluations of suspension snow flux and blowing snow occurrence using observed wind fields to drive SnowPappus were also performed. They show that SnowPappus is able to simulate reasonable average suspension fluxes if the effective terminal fall speed of suspended snow particles is adequately calibrated, and that blowing snow occurrence is satisfactorily captured. However, the simulation outputs have a strong uncertainty, which is coherent with previous results obtained with other models. Numerous badly known physical parameters and understudied parameters limit improvements of the used parameterizations. Moreover, uncertainty linked to parameterization combines with uncertainties in forcing wind speed. Therefore, it may lead to local fluxes being strongly different from the simulated one. They will have to be understood more as a "first guess" than as a quantitative estimate.

Future work will include an evaluation of the simulated snow spatial distribution against satellite data (snow depth maps from satellite stereo imagery, snow cover maps for satellite optical imagery, ...). Depending on the results of these future studies, various improvements of SnowPappus could be done, such as representing the effect of subgrid topography on transport fluxes (Bowling et al., 2004) or testing different parameterization of deposited snow properties. Finally, the high and partly unavoidable uncertainty in the simulation outputs also stresses the need to include ensemble simulations and data assimilation in the future system.

Code and data availability. The SnowPappus blowing snow model is developed in the framework of the open-source SURFEX project. The source files of SURFEX code are provided at https://doi.org/10.5281/zenodo.7687821 to guarantee the permanent reproducibility of results. However, we recommend that potential future users and developers access to the code from its Git repository (http://git.umr-cnrm.fr/git/Surfex_Git2.git, last access: 1 mars 2023) to benefit from all tools of code management (history management, bug fixes, documentation, interface for technical support, etc.). This requires a quick registration, and the procedure is described at https://opensource.umr-cnrm.fr/projects/snowtools_git/wiki/Install_SURFEX (last access: 1 mars 2023). The version used in this work is tagged as SnowPappus-v1.0. A user manual, describing the SURFEX namelist options related to SnowPappus is available at https://doi.org/10.5281/zenodo.7681340. More general information about SURFEX use can be found at https://opensource.umr-cnrm.fr/projects/snowtools_git/wiki and https://opensource.umr-cnrm.fr/projects/snowtools_git/wiki (last accesses: 1 mars 2023) The DEM used in this study originate from RGE Alti® website. They can be downloaded freely at https://geoservices.ign.fr/documentation/donnees/alti/rgealti. ISAW Network stations raw data are freely available on http://iav-portal.com/index.php?nav=iodmisawlist&lang=en&search=&center=&sort_field=center&sort_asc=1. The data from *Col du Lac Blanc* station is available at https://doi.org/10.17178/CRYOBSCLIM.CLB.COL.csv and are described by Guyomarc'h et al. (2019). AROME downscaled wind forcing used for simulations on Grandes Rousses test zone is available at https://doi.org/10.5281/zenodo.7681661. Input data , namelists and instructions to run the model and produce most of the plots and simulations presented in this paper are available for download at https://doi.org/10.5281/zenodo.7681551. In the same folder, codes generating some additional results not shown in the article are available (see Sect. 4.5 and 6.1)

Appendix A: Supplementary figures

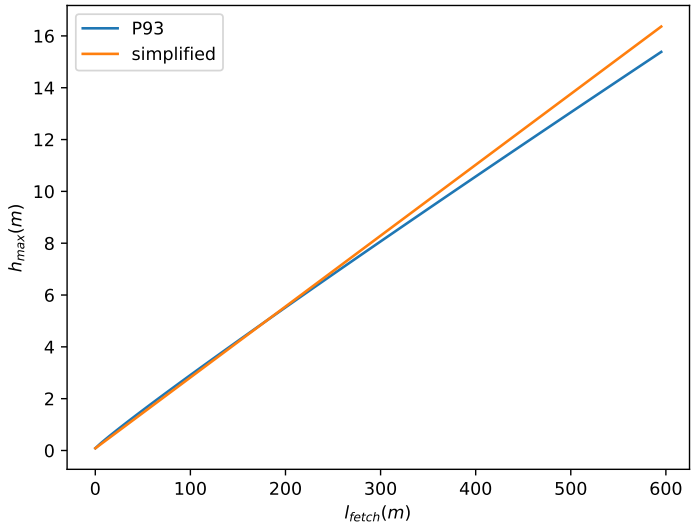

Figure A1. Comparison between the height h_{max} given in Sect. 3.3.2 used as an upper bound for suspension transport (blue curve) and the one computed with Eq. 10 from Pomeroy et al. (1993) (orange curve). Both heights are plotted as a function of the fetch distance as defined in Sect. 3.3.2.

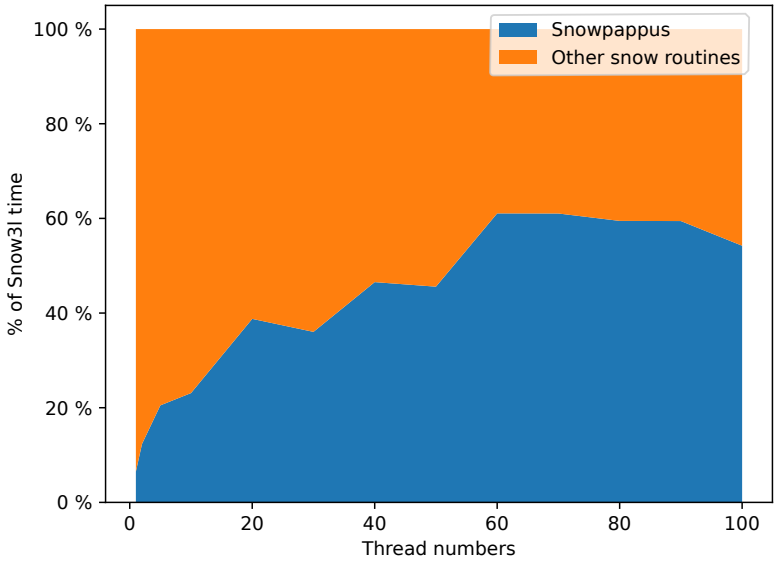

Figure A2. Visualisation of the proportion of time spent in the SnowPappus routine among all snow-related routines ('Full Snow routine' Fig. 4) computing time.

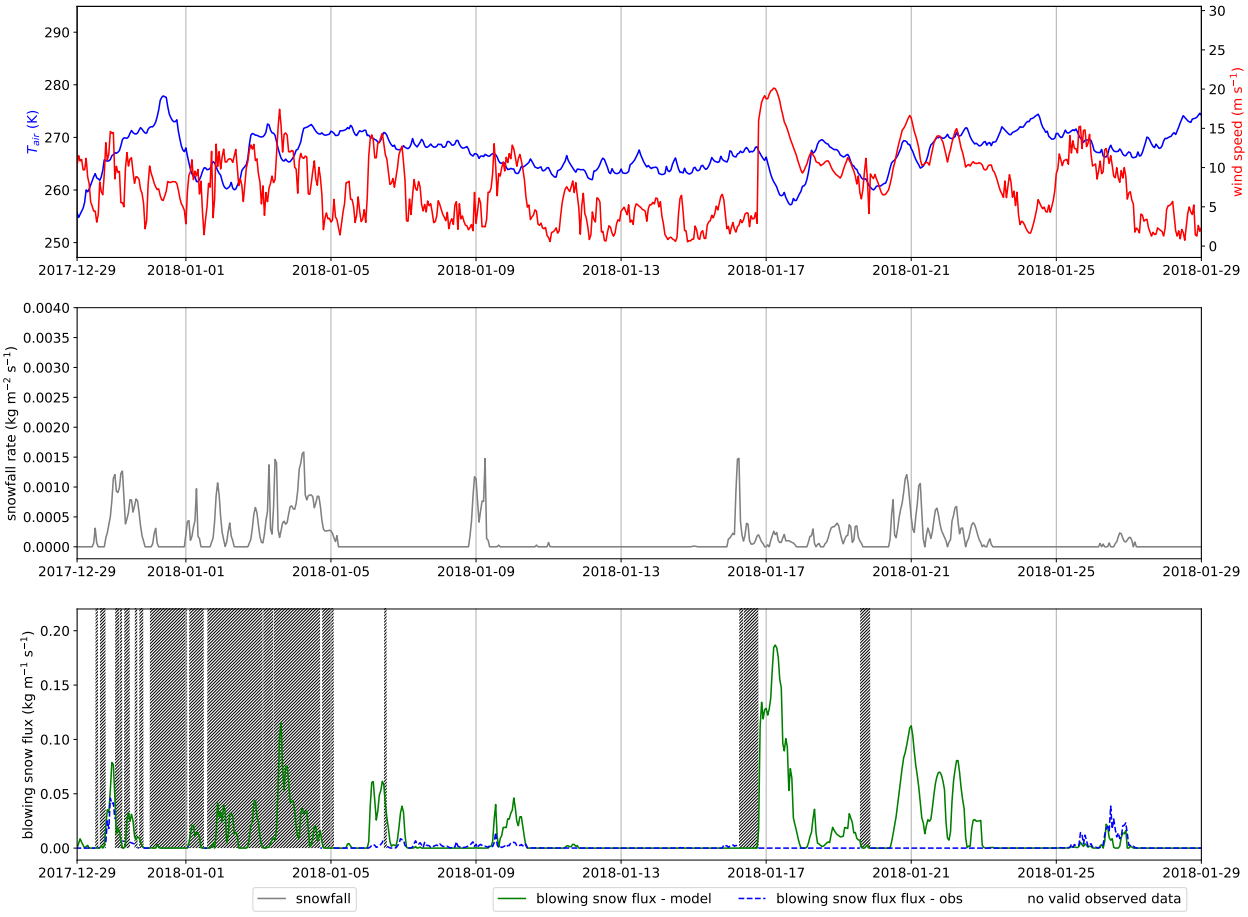

Figure A3. Modelled and SPC-measured 0.2 -1.2 m blowing snow flux during January 2018. SAFRAN-modelled air temperature and solid precipitations, as well as measured wind speed are also represented. This month is a clear outlier in the comparison between observed and modelled fluxes presented in Fig. 12. Here we see that, during the two main modelled events of the month (17 January and 21 January), no flux is detected by the SPC, despite high wind (15-20 m s^{-1}) , negative temperatures in the previous weeks, preventing the formation of an ice crust, and co-occurring heavy snowfall, which should bring continuously transportable snow. It seems to indicate either an undetected SPC deficiency or big errors in the forcing fields during this month, rather than a model failure.

Appendix B: Maximum height of the suspension layer

Following Pomeroy et al. (1993), we assume the maximum height reached by particles in the suspension layer is limited by the time available to diffuse t_d, so that $h_{max} = ku_* t_d$. Consequently, suspension transport grows with fetch distance. In SnowPappus, we additionally assume this is valid no matter the fetch distance. We also simplified the expression used by Pomeroy et al. (1993) to get an analytical expression, obtaining $h_{max} = h_{salt} + \frac{k^2}{\sqrt{log(\frac{h_{salt}}{z0})log(\frac{5m}{z_0})}}$. Appendix Fig. A1 compares the exact and approximated formula, and shows their difference is small. This approach assumes an abrupt end of the suspension layer at the height h_{max}, which is not realistic. However it influences the model outputs only if a significant flux would occur above h_{max}. We can show it happens only when wind speed exceeds 30-40 m s^{-1} (γ becomes lower than 1, making the flux profile not integrable) or if h_{max} is inferior to $\approx$ 30 cm, when $l_{fetch} < 10 - 20$ m.

Appendix C: Expression of F(T)

$F(T)$ used in Eq. 17 is expressed as follows (Essery et al., 1999) :

$$F(T) = \frac{L_s}{\lambda_T T}(\frac{L_s M}{RT} - 1) + \frac{1}{D\rho_s} \tag{C1}$$

with T the air temperature (K), L_s the latent heat of ice sublimation, M the molar mass of water (kg.mol^{-1}), R the universal gas constant (J.K^{-1}.mol^{-1}), ρ_s is the water vapour saturation density (kg.m^{-3}).

Appendix D: Conversion formula between old and new Crocus microstructure formalism

In the current version of SURFEX, the microstructure of Crocus is described with two prognostic variables : the optical diameter D_{opt} and the sphericity s. In this article, we often refer to the dendricity d and grain size g_s which were used in older versions of Crocus (Vionnet et al., 2012). Carmagnola et al. (2014) proposed formulas linking D_{opt}, s, g_s and d. However some errors were detected in this work, leading us to use another formula to get grain size from D_{opt} and s. This formula is presented here:

$$g_s = 2\frac{D_{opt} - 2\alpha(1-s)}{1+s} \tag{D1}$$

The formula from Carmagnola et al. (2014) is used to compute the dendricity d from s and D_{opt}. Details about this new conversions formulas and their impact on Crocus metamorphism will be described in a paper in preparation.

Appendix E: Properties of deposited snow in case of simultaneous snowfall and wind-driven redeposition

We consider here the case when during a time step, a mass m_{SP} and m_{BS} (kg m^{-2}) of snow coming respectively from solid precipitation and wind-driven redeposition has to be added to the snowpack during a simulation time step. Optical diameter

D_{BS} and sphericity s_{BS} sphericity s_{BS} of the deposited wind-blown snow are given in Sect. 3.6. Solid precipitation sphericity s_{SP} and optical diameter D_{SP} are computed as in the default Crocus configuration, described in Vionnet et al. (2012). In this case, a layer of total mass $m = m_{\mathrm{SP}} + m_{\mathrm{BS}}$ is added to the snowpack. Its properties s and D are given by the weighted average of blowing snow and solid precipitation properties:

$$s = \frac{m_{\mathrm{SP}} s_{\mathrm{SP}} + m_{\mathrm{BS}} s_{\mathrm{BS}}}{m_{\mathrm{SP}} + m_{\mathrm{BS}}} \tag{E1}$$

$$D = \frac{m_{\mathrm{SP}} D_{\mathrm{SP}} + m_{\mathrm{BS}} D_{\mathrm{BS}}}{m_{\mathrm{SP}} + m_{\mathrm{BS}}} \tag{E2}$$

Author contributions. A.H. and M.B. developed jointly the SnowPappus code with equal contribution. A.H. had a special involvement in coding the mass balance routine and MPI parallelization. M.B. redacted the introduction, discussion and conclusion of the article. He surveyed the bibliography, and made theoretical choices and most of the technical work concerning saltation and suspension snow flux simulations, and general evaluation of the model. A.H. did it for mass balance, sublimation and numerical performance tests. M.L. supervised the work, provided technical support on Crocus and SURFEX, ran Sytron simulations and was extensively involved in the proofreading process. L.LT provided wind forcing for the two-dimensional simulation and helped in writing the article. V.V. participated in theoretical discussions, in particular about Sytron, and proofread the article. M.F. participated in debugging and helped code development.

Competing interests. The authors declare that they have no conflict of interest.

Acknowledgements. This work was conducted using mainly Meteo France office and computing ressource. Main fundings are SENSASS project funded by the Region Auvergne Rhône-Alpes (France) and CDSN PhD grant. We thank **Hervé Bellot** for providing Blowing snow flux data at col du Lac Blanc, as well as **Yannick Deliot**, **Hugo Merzisen** and **Isabelle Gouttevin** who provided advice and technical information about their use and about *Col du Lac Blanc* experimental site in general. We also thank **Rafife Nheili** for her help and participation in coding the MPI parallelization routine. Generally, we thank the whole Centre d'Etude de la Neige modelling team, for multiple fruitful discussions and diverse technical support. CNRM/CEN and LECA are part of LabEx OSUG@2020.

References

Aksamit, N. O. and Pomeroy, J. W.: The Effect of Coherent Structures in the Atmospheric Surface Layer on Blowing-Snow Transport, Boundary-Layer Meteorology, https://doi.org/10.1007/s10546-017-0318-2, 2017.

Amory, C., Kittel, C., Le Toumelin, L., Agosta, C., Delhasse, A., Favier, V., and Fettweis, X.: Performance of MAR (v3. 11) in simulating the drifting-snow climate and surface mass balance of Adélie Land, East Antarctica, Geoscientific Model Development, 14, 3487–3510, https://doi.org/0.5194/gmd-14-3487-2021, 2021.

Baba, M. W., Gascoin, S., Kinnard, C., Marchane, A., and Hanich, L.: Effect of Digital Elevation Model Resolution on the Simulation of the Snow Cover Evolution in the High Atlas, Water Resources Research, 55, 5360–5378, https://doi.org/10.1029/2018wr023789, 2019.

Bartelt, P. and Lehning, M.: A physical SNOWPACK model for the Swiss avalanche warning: Part I: numerical model, Cold Regions Science and Technology, 35, 123–145, https://doi.org/10.1016/S0165-232X(02)00074-5, 2002.

Bernhardt, M., Zängl, G., Liston, G., Strasser, U., and Mauser, W.: Using wind fields from a high-resolution atmospheric model for simulating snow dynamics in mountainous terrain, Hydrological Processes: An International Journal, 23, 1064–1075, https://doi.org/10.1002/hyp.7208, 2009.

Bintanja, R.: Snowdrift suspension and atmospheric turbulence. Part I: Theoretical background and model description, Boundary-layer meteorology, 95, 343–368, https://doi.org/10.1023/A:1002676804487, 2000.

Bowling, L., Pomeroy, J., and Lettenmaier, D.: Parameterization of blowing-snow sublimation in a macroscale hydrology model, Journal of Hydrometeorology, 5, 745–762, https://doi.org/10.1175/1525-7541(2004)005%3C0745:POBSIA%3E2.0.CO;2, 2004.

Brousseau, P., Seity, Y., Ricard, D., and Léger, J.: Improvement of the forecast of convective activity from the AROME-France system, Quarterly Journal of the Royal Meteorological Society, 142, 2231–2243, https://doi.org/10.1002/qj.2822, 2016.

Carmagnola, C., Morin, S., Lafaysse, M., Domine, F., Lesaffre, B., Lejeune, Y., Picard, G., and Arnaud, L.: Implementation and evaluation of prognostic representations of the optical diameter of snow in the SURFEX/ISBA-Crocus detailed snowpack model, The Cryosphere, 8, 417–437, https://doi.org/10.5194/tc-8-417-2014, 2014.

Castelle, T., Sivardiere, F., Guyomarc'H, G., Buisson, L., and Mérindol, L.: Drifting zone phenomena and avalanches, in: International symposium on snow and related manifestations, Manali, IND, September 1994, p. 7, 1994.

Choler, P.: Growth response of temperate mountain grasslands to inter-annual variations in snow cover duration, Biogeosciences, 12, 3885–3897, https://doi.org/10.5194/bg-12-3885-2015, 2015.

Chritin, V., Bolognesi, R., and Gubler, H.: FlowCapt: a new acoustic sensor to measure snowdrift and wind velocity for avalanche forecasting, Cold Regions Science and Technology, 30, 125–133, https://doi.org/10.1016/S0165-232X(99)00012-9, 1999.

Cierco, F.-X., Naaim-Bouvet, F., and Bellot, H.: Acoustic sensors for snowdrift measurements: How should they be used for research purposes?, Cold Regions Science and Technology, 49, 74–87, https://doi.org/10.1016/j.coldregions.2007.01.002, 2007.

Clarke, L., Glendinning, I., and Hempel, R.: The MPI message passing interface standard, in: Programming environments for massively parallel distributed systems, pp. 213–218, Springer, https://doi.org/10.1007/978-3-0348-8534-8_21, 1994.

Clifton, A., Rüedi, J.-D., and Lehning, M.: Snow saltation threshold measurements in a drifting-snow wind tunnel, Journal of Glaciology, 52, 585–596, https://doi.org/10.3189/172756506781828430, 2006.

Cluzet, B., Lafaysse, M., Deschamps-Berger, C., Vernay, M., and Dumont, M.: Propagating information from snow observations with CrocO ensemble data assimilation system: a 10-years case study over a snow depth observation network., Cryosphere Discussions, https://doi.org/10.5194/tc-16-1281-2022, 2021.

Comola, F. and Lehning, M.: Energy-and momentum-conserving model of splash entrainment in sand and snow saltation, Geophysical Research Letters, 44, 1601–1609, https://doi.org/10.1002/2016GL071822, 2017.

Comola, F., Kok, J. F., Gaume, J., Paterna, E., and Lehning, M.: Fragmentation of wind-blown snow crystals, Geophysical Research Letters, 44, 4195–4203, https://doi.org/10.1002/2017GL073039, 2017.

Déry, S. J. and Yau, M.: A bulk blowing snow model, Boundary-Layer Meteorology, 93, 237–251, https://doi.org/10.1023/A:1002065615856, 1999.

Déry, S. J. and Yau, M.: Simulation of blowing snow in the Canadian Arctic using a double-moment model, Boundary-Layer Meteorology, 99, 297–316, https://doi.org/10.1023/A:1018965008049, 2001.

Deschamps-Berger, C., Cluzet, B., Dumont, M., Lafaysse, M., Berthier, E., Fanise, P., and Gascoin, S.: Improving the spatial distribution of snow cover simulations by assimilation of satellite stereoscopic imagery, Water Resources Research, 58, e2021WR030 271, https://doi.org/10.1029/2021WR030271, 2022.

Doorschot, J. J. and Lehning, M.: Equilibrium saltation: mass fluxes, aerodynamic entrainment, and dependence on grain properties, Boundary-Layer Meteorology, 104, 111–130, https://doi.org/10.1023/A:1015516420286, 2002.

Doorschot, J. J., Lehning, M., and Vrouwe, A.: Field measurements of snow-drift threshold and mass fluxes, and related model simulations, Boundary-Layer Meteorology, 113, 347–368, 2004.

Dujardin, J. and Lehning, M.: Wind-Topo: Downscaling near-surface wind fields to high-resolution topography in highly complex terrain with deep learning, Quarterly Journal of the Royal Meteorological Society, 148, 1368–1388, https://doi.org/10.1002/qj.4265, 2022.

Essery, R., Li, L., and Pomeroy, J.: A distributed model of blowing snow over complex terrain, Hydrological processes, 13, 2423–2438, https://doi.org/10.1002/(SICI)1099-1085(199910)13:14/15%3C2423::AID-HYP853%3E3.0.CO;2-U, 1999.

Gallée, H., Guyomarc'h, G., and Brun, E.: Impact of snow drift on the Antarctic ice sheet surface mass balance: possible sensitivity to snow-surface properties, Boundary-Layer Meteorology, 99, 1–19, https://doi.org/10.1023/A:1018776422809, 2001.

Gordon, M., Simon, K., and Taylor, P. A.: On snow depth predictions with the Canadian land surface scheme including a parametrization of blowing snow sublimation, Atmosphere-Ocean, 44, 239–255, https://doi.org/10.3137/ao.440303, 2006.

Gordon, M., Savelyev, S., and Taylor, P. A.: Measurements of blowing snow, part II: Mass and number density profiles and saltation height at Franklin Bay, NWT, Canada, Cold Regions Science and Technology, 55, 75–85, https://doi.org/10.1016/j.coldregions.2008.07.001, 2009.

Greenshields, C. and Weller, H.: Notes on Computational Fluid Dynamics: General Principles, CFD Direct Ltd, Reading, UK, 2022.

Groot Zwaaftink, C., Diebold, M., Horender, S., Overney, J., Lieberherr, G., Parlange, M., and Lehning, M.: Modelling small-scale drifting snow with a Lagrangian stochastic model based on large-eddy simulations, Boundary-Layer Meteorology, 153, 117–139, https://doi.org/10.1007/s10546-014-9934-2, 2014.

Grünewald, T., Schirmer, M., Mott, R., and Lehning, M.: Spatial and temporal variability of snow depth and ablation rates in a small mountain catchment, The Cryosphere, 4, 215–225, https://doi.org/10.5194/tc-4-215-2010, 2010.

Guyomarc'h, G., Bellot, H., Vionnet, V., Naaim-Bouvet, F., Déliot, Y., Fontaine, F., Puglièse, P., Nishimura, K., Durand, Y., and Naaim, M.: A meteorological and blowing snow data set (2000–2016) from a high-elevation alpine site (Col du Lac Blanc, France, 2720 m asl), Earth System Science Data, 11, 57–69, https://doi.org/10.5194/essd-11-57-2019, 2019.

Guyomarc'h, G. and Mérindol, L.: Validation of an application for forecasting blowing snow, Annals of Glaciology, 26, 138–143, https://doi.org/10.3189/1998AoG26-1-138-143, 1998.

He, S. and Ohara, N.: A New Formula for Estimating the Threshold Wind Speed for Snow Movement, Journal of Advances in Modeling Earth Systems, 9, 2514–2525, https://doi.org/10.1002/2017ms000982, 2017.

Helbig, N., Mott, R., Van Herwijnen, A., Winstral, A., and Jonas, T.: Parameterizing surface wind speed over complex topography, Journal of Geophysical Research: Atmospheres, 122, 651–667, https://doi.org/10.1002/2016JD025593, 2017.

Helfricht, K., Hartl, L., Koch, R., Marty, C., and Olefs, M.: Obtaining sub-daily new snow density from automated measurements in high mountain regions, Hydrology and Earth System Sciences, 22, 2655–2668, https://doi.org/10.5194/hess-22-2655-2018, 2018.

IPCC: The Ocean and Cryosphere in a Changing Climate, Cambridge University Press, https://doi.org/10.1017/9781009157964, 2022.

Jordan, R. E.: A one-dimensional temperature model for a snow cover: Technical documentation for SNTHERM. 89, 1991.

Kind, R.: One-dimensional aeolian suspension above beds of loose particles—A new concentration-profile equation, Atmospheric Environment. Part A. General Topics, 26, 927–931, 1992.

Lafaysse, M.: Modélisation numérique de la neige : la fin du déterminisme ?, Habilitation à diriger des recherches, Université Toulouse III - Paul Sabatier, https://hal.science/tel-04130109, 2023.

Largeron, C., Dumont, M., Morin, S., Boone, A., Lafaysse, M., Metref, S., Cosme, E., Jonas, T., Winstral, A., and Margulis, S. A.: Toward snow cover estimation in mountainous areas using modern data assimilation methods: a review, Frontiers in Earth Science, 8, 325, https://doi.org/10.3389/feart.2020.00325, 2020.

Le Toumelin, L., Gouttevin, I., Helbig, N., Galiez, C., Roux, M., and Karbou, F.: Emulating the adaptation of wind fields to complex terrain with deep-learning, Artificial Intelligence for the Earth Systems, pp. 1–39, https://doi.org/10.1175/AIES-D-22-0034.1, 2022.

Lehning, M., Doorschot, J., and Bartelt, P.: A snowdrift index based on SNOWPACK model calculations, Annals of Glaciology, 31, 382–386, https://doi.org/10.3189/172756400781819770, 2000.

Lehning, M., Löwe, H., Ryser, M., and Raderschall, N.: Inhomogeneous precipitation distribution and snow transport in steep terrain, Water Resources Research, 44, https://doi.org/10.1029/2007WR006545, 2008.

Li, L. and Pomeroy, J. W.: Estimates of threshold wind speeds for snow transport using meteorological data, Journal of Applied Meteorology, 36, 205–213, https://doi.org/10.1175/1520-0450(1997)036<0205:EOTWSF>2.0.CO;2, 1997.

Liston, G. E. and Sturm, M.: A snow-transport model for complex terrain, Journal of Glaciology, 44, 498–516, https://doi.org/10.3189/S0022143000002021, 1998.

Liston, G. E., Haehnel, R. B., Sturm, M., Hiemstra, C. A., Berezovskaya, S., and Tabler, R. D.: Simulating complex snow distributions in windy environments using SnowTran-3D, Journal of Glaciology, 53, 241–256, https://doi.org/10.3189/172756507782202865, 2007.

MacDonald, M. K., Pomeroy, J. W., and Pietroniro, A.: Parameterizing redistribution and sublimation of blowing snow for hydrological models: tests in a mountainous subarctic catchment, Hydrological Processes: An International Journal, 23, 2570–2583, https://doi.org/10.1002/hyp.7356, 2009.

Mann, G., Anderson, P., and Mobbs, S.: Profile measurements of blowing snow at Halley, Antarctica, Journal of Geophysical Research: Atmospheres, 105, 24 491–24 508, https://doi.org/10.1029/2000JD900247, 2000.

Marsh, C. B., Pomeroy, J. W., Spiteri, R. J., and Wheater, H. S.: A finite volume blowing snow model for use with variable resolution meshes, Water Resources Research, 56, e2019WR025 307, https://doi.org/10.1029/2019WR025307, 2020.

Melo, D. B., Sharma, V., Comola, F., Sigmund, A., and Lehning, M.: Modeling snow saltation: the effect of grain size and interparticle cohesion, Journal of Geophysical Research: Atmospheres, 127, e2021JD035 260, https://doi.org/10.1029/2021JD035260, 2022.

Michaux, J.-L.: Etude, compréhension, et modélisation des phénomènes liés au transport de la neige par le vent, Ph.D. thesis, Doctorat Environnement risques naturels, Université Joseph Fourier, Grenoble, 2003.

Morin, S., Horton, S., Techel, F., Bavay, M., Coléou, C., Fierz, C., Gobiet, A., Hagenmuller, P., Lafaysse, M., Ližar, M., Mitterer, C., Monti, F., Müller, K., Olefs, M., Snook, J. S., van Herwijnen, A., and Vionnet, V.: Application of physical snowpack models in support of

operational avalanche hazard forecasting: A status report on current implementations and prospects for the future, Cold Regions Science and Technology, 170, 102 910, https://doi.org/10.1016/j.coldregions.2019.102910, 2020a.

Morin, S., Horton, S., Techel, F., Bavay, M., Coléou, C., Fierz, C., Gobiet, A., Hagenmuller, P., Lafaysse, M., Ližar, M., et al.: Application of physical snowpack models in support of operational avalanche hazard forecasting: A status report on current implementations and prospects for the future, Cold regions science and technology, 170, 102 910, https://doi.org/10.1016/j.coldregions.2019.102910, 2020b.

Mott, R., Vionnet, V., and Grünewald, T.: The seasonal snow cover dynamics: review on wind-driven coupling processes, Frontiers in Earth Science, 6, 197, https://doi.org/10.3389/feart.2018.00197, 2018.

Musselman, K. N., Pomeroy, J. W., Essery, R. L., and Leroux, N.: Impact of windflow calculations on simulations of alpine snow accumulation, redistribution and ablation, Hydrological Processes, 29, 3983–3999, https://doi.org/10.1002/hyp.10595, 2015.

Naaim-Bouvet, F., Naaim, M., and Martinez, H.: Profils de concentration de la neige soufflée. Théorie, résolution numérique et validation expérimentale in situ, La Houille Blanche, pp. 53–56, https://doi.org/10.1051/lhb/1996052, 1996.

Naaim-Bouvet, F., Bellot, H., and Naaim, M.: Back analysis of drifting-snow measurements over an instrumented mountainous site, Annals of Glaciology, 51, 207–217, https://doi.org/10.3189/172756410791386661, 2010.

Nemoto, M. and Nishimura, K.: Numerical simulation of snow saltation and suspension in a turbulent boundary layer, Journal of Geophysical Research: Atmospheres, 109, https://doi.org/10.1029/2004JD004657, 2004.

Nishimura, K. and Hunt, J.: Saltation and incipient suspension above a flat particle bed below a turbulent boundary layer, Journal of Fluid Mechanics, 417, 77–102, https://doi.org/10.1017/S0022112000001014, 2000.

Patankar, S. V.: Numerical heat transfer and fluid flow, CRC press, https://doi.org/10.1201/9781482234213, 2018.

Pomeroy, J. and Gray, D.: Saltation of snow, Water resources research, 26, 1583–1594, https://doi.org/10.1029/WR026i007p01583, 1990.

Pomeroy, J. and Male, D.: Steady-state suspension of snow, Journal of hydrology, 136, 275–301, https://doi.org/10.1016/0022-1694(92)90015-N, 1992.

Pomeroy, J., Gray, D., and Landine, P.: The prairie blowing snow model: characteristics, validation, operation, Journal of Hydrology, 144, 165–192, https://doi.org/10.1016/0022-1694(93)90171-5, 1993.

Pomeroy, J., Gray, D., Brown, T., Hedstrom, N., Quinton, W., Granger, R., and Carey, S.: The cold regions hydrological model: a platform for basing process representation and model structure on physical evidence, Hydrological Processes: An International Journal, 21, 2650–2667, https://doi.org/10.1002/hyp.6787, 2007.

Raderschall, N., Lehning, M., and Schär, C.: Fine-scale modeling of the boundary layer wind field over steep topography, Water Resources Research, 44, https://doi.org/10.1029/2007WR006544, 2008.

Revuelto, J., Lecourt, G., Lafaysse, M., Zin, I., Charrois, L., Vionnet, V., Dumont, M., Rabatel, A., Six, D., Condom, T., et al.: Multi-criteria evaluation of snowpack simulations in complex alpine terrain using satellite and in situ observations, Remote Sensing, 10, 1171, https://doi.org/10.3390/rs10081171, 2018.

Saarinen, S., Hamrud, M., Salmond, D., and Hague, J.: Dr. hook instrumentation tool, 2005.

Sato, T., Kimura, T., Ishimaru, T., and Maruyama, T.: Field test of a new snow-particle counter (SPC) system, Annals of Glaciology, 18, 149–154, https://doi.org/10.3189/S0260305500011411, 1993.

Sato, T., Mochizuki, S., Kosugi, K., and Nemoto, M.: Effects of particle shape on mass flux measurement of drifting snow by snow particle counter, Journal of the Japanese Society of Snow and Ice, 67, 493–503, https://doi.org/10.5331/seppyo.67.493, 2005.

Sato, T., Kosugi, K., Mochizuki, S., and Nemoto, M.: Wind speed dependences of fracture and accumulation of snowflakes on snow surface, Cold Regions Science and Technology, 51, 229–239, https://doi.org/10.1016/j.coldregions.2007.05.004, 2008.

SBSM: Code documentation, https://documentation.help/CRHM_Borland/modules_sbsm.htm, accessed: 2022-06-04.

Schmidt, D. S., Schmidt, R., and Dent, J.: Electrostatic force in blowing snow, Boundary-Layer Meteorology, 93, 29–45, https://doi.org/10.1023/A:1002045818907, 1999.

Schmidt, R.: Threshold wind-speeds and elastic impact in snow transport, Journal of Glaciology, 26, 453–467, https://doi.org/10.1017/S0022143000010972, 1980.

Schneiderbauer, S. and Prokop, A.: The atmospheric snow-transport model: SnowDrift3D, Journal of Glaciology, 57, 526–542, https://doi.org/10.3189/002214311796905677, 2011a.

Schneiderbauer, S. and Prokop, A.: The atmospheric snow-transport model: SnowDrift3D, Journal of Glaciology, 57, 526–542, https://doi.org/10.3189/002214311796905677, 2011b.

Schweizer, J., Jamieson, J. B., and Schneebeli, M.: Snow avalanche formation, Reviews of Geophysics, 41, https://doi.org/10.1029/2002rg000123, 2003.

Seity, Y., Brousseau, P., Malardel, S., Hello, G., Bénard, P., Bouttier, F., Lac, C., and Masson, V.: The AROME-France convective-scale operational model, Monthly Weather Review, 139, 976–991, https://doi.org/10.1175/2010MWR3425.1, 2011.

Shao, Y.: A similarity theory for saltation and application to aeolian mass flux, Boundary-layer meteorology, 115, 319–338, https://doi.org/10.1007/s10546-004-4632-0, 2005.

Sharma, V., Gerber, F., and Lehning, M.: Introducing CRYOWRF v1. 0: Multiscale atmospheric flow simulations with advanced snow cover modelling, Geoscientific Model Development Discussions, pp. 1–46, https://doi.org/10.5194/gmd-2021-231, 2021.

Sommer, C. G., Lehning, M., and Fierz, C.: Wind Tunnel Experiments: Influence of Erosion and Deposition on Wind-Packing of New Snow, Frontiers in Earth Science, 6, https://doi.org/10.3389/feart.2018.00004, 2018.

Sørensen, M.: On the rate of aeolian sand transport, Geomorphology, 59, 53–62, https://doi.org/10.1016/j.geomorph.2003.09.005, 2004.

Takahashi, S.: Characteristics of drifting snow at Mizuho Station, Antarctica, Annals of glaciology, 6, 71–75, https://doi.org/10.3189/1985AoG6-1-71-75, 1985.

Trouvilliez, A., Naaim-Bouvet, F., Bellot, H., Genthon, C., and Gallée, H.: Evaluation of the FlowCapt acoustic sensor for the aeolian transport of snow, Journal of Atmospheric and Oceanic Technology, 32, 1630–1641, https://doi.org/10.1175/JTECH-D-14-00104.1, 2015.

Vernay, M., Lafaysse, M., Monteiro, D., Hagenmuller, P., Nheili, R., Samacoïts, R., Verfaillie, D., and Morin, S.: The S2M meteorological and snow cover reanalysis over the French mountainous areas: description and evaluation (1958–2021), Earth System Science Data, 14, 1707–1733, https://doi.org/10.5194/essd-14-1707-2022, 2022.

Vionnet, V.: Études du transport de la neige par le vent en conditions alpines: observations et simulations à l'aide d'un modèle couplé atmosphère/manteau neigeux, Ph.D. thesis, Paris Est, 2012.

Vionnet, V., Brun, E., Morin, S., Boone, A., Faroux, S., Le Moigne, P., Martin, E., and Willemet, J.-M.: The detailed snowpack scheme Crocus and its implementation in SURFEX v7. 2, Geoscientific Model Development, 5, 773–791, https://doi.org/10.5194/gmd-5-773-2012, 2012.

Vionnet, V., Guyomarc'h, G., Bouvet, F. N., Martin, E., Durand, Y., Bellot, H., Bel, C., and Puglièse, P.: Occurrence of blowing snow events at an alpine site over a 10-year period: Observations and modelling, Advances in water resources, 55, 53–63, https://doi.org/10.1016/j.advwatres.2012.05.004, 2013.

Vionnet, V., Martin, E., Masson, V., Guyomarc'h, G., Naaim-Bouvet, F., Prokop, A., Durand, Y., and Lac, C.: Simulation of wind-induced snow transport and sublimation in alpine terrain using a fully coupled snowpack/atmosphere model, The Cryosphere, 8, 395–415, https://doi.org/10.5194/tc-8-395-2014, 2014.

Vionnet, V., Dombrowski-Etchevers, I., Lafaysse, M., Quéno, L., Seity, Y., and Bazile, E.: Numerical weather forecasts at kilometer scale in the French Alps: Evaluation and application for snowpack modeling, Journal of Hydrometeorology, 17, 2591–2614, https://doi.org/10.1175/JHM-D-15-0241.1, 2016.

Vionnet, V., Martin, E., Masson, V., Lac, C., Naaim Bouvet, F., and Guyomarc'h, G.: High-resolution large eddy simulation of snow accumulation in Alpine terrain, Journal of Geophysical Research: Atmospheres, 122, 11–005, https://doi.org/10.1002/2017JD026947, 2017.

Vionnet, V., Guyomarc'h, G., Lafaysse, M., Naaim-Bouvet, F., Giraud, G., and Deliot, Y.: Operational implementation and evaluation of a blowing snow scheme for avalanche hazard forecasting, Cold Regions Science and Technology, 147, 1–10, https://doi.org/10.1016/j.coldregions.2017.12.006, 2018.

White, B. R. and Tsoar, H.: Slope effect on saltation over a climbing sand dune, Geomorphology, 22, 159–180, https://doi.org/10.1016/S0169-555X(97)00058-5, 1998.

Wilcox, R.: A note on the Theil-Sen regression estimator when the regressor is random and the error term is heteroscedastic, Biometrical Journal: Journal of Mathematical Methods in Biosciences, 40, 261–268, https://doi.org/10.1002/(SICI)1521-4036(199807)40:3%3C261::AID-BIMJ261%3E3.0.CO;2-V, 1998.

Xue, M., Droegemeier, K. K., and Wong, V.: The Advanced Regional Prediction System (ARPS)–A multi-scale nonhydrostatic atmospheric simulation and prediction model. Part I: Model dynamics and verification, Meteorology and atmospheric physics, 75, 161–193, https://doi.org/10.1007/s007030070003, 2000.

Yang, J. and Yau, M.: A new triple-moment blowing snow model, Boundary-layer meteorology, 126, 137–155, https://doi.org/10.1007/s10546-007-9215-4, 2008.